SESSION 4

NONLINEAR EFFECTS

Session Chairman:

Robert E. Fulton

Aerospace Engineer, NASA Langley
Research Center, Hampton, Virginia

MATRIX ANALYSIS METHODS FOR INELASTIC STRUCTURES

W. Lansing*
W. R. Jensen**
W. Falby**

Grumman Aircraft Engineering Corporation
Bethpage, New York

A review is presented of one of the methods proposed in the literature for predicting the influence of plasticity in redundant structures. It is essentially a step by step calculation procedure, and corresponds to the flow theory of plasticity. The method has been introduced into a standard, initial strain influence coefficient formulation and applied to a 2024-T4 aluminum alloy shear lag structure which has been tested previously for the Air Force. The resulting correlation between predicted and test results is reasonably good. The computer program has also been modified to yield a deformation theory solution for the same structure; the numerical results are extremely close to those of the flow theory. In addition to this, primary creep is considered; the predicted strain distributions in an 1100-F aluminum shear lag structure again agree reasonably well with test values. Finally, it is observed that in all these cases the calculation step size is vitally important, and a simple, straight forward procedure is recommended as a check.

SYMBOLS

σ_u	u^{th} ordinary stress component (normal or shear) at a node point
$\sigma_{3N-2}, \sigma_{3N-1}, \sigma_{3N}$	The normal stress components and shear stress component at node N - another designation for σ_u
$\bar{\sigma}_N$	Effective stress at node N
σ_o	Reference stress in Ramberg-Osgood equation
Γ_{um}	u^{th} stress component in linear redundant structure due to the m^{th} unit applied load
Γ_{uv}	u^{th} stress component in linear redundant structure due to the v^{th} unit initial strain

Work described in this paper was sponsored in part, by the Air force Flight Dynamics Laboratory, RTD, USAF, under contract No. AF 33(615)-2260. A portion of the work had previously been completed under the sponsorship of the Grumman Aircraft Engineering Corporation Advanced Development Program.

* Chief of Structural Mechanics

** Structural Methods Engineers

P_m	m^{th} applied load
ϵ_v	v^{th} component of initial strain
$\epsilon(p)_v$	v^{th} component of plastic strain
$\epsilon(c)_v$	v^{th} component of creep strain
$\bar{\epsilon}(p)_N$	Effective plastic strain at node N
$\bar{\epsilon}(c)_N$	Effective creep strain at node N
$\mathcal{E}$	Total (elastic, plastic and creep) strain component
t^*	Equivalent time at start of cycle
Δt	Cycle duration (elapsed time)
α, β, γ	Material constants in creep strain equation
Δ	Increment (prefix)
θ	Nonlinear parameter in Ramberg-Osgood equation
k	Cycle designation, superscript

INTRODUCTION

The problem of determining the stress distributions in structures subject to plasticity and creep is highly nonlinear. This fact has long made it very difficult to obtain solutions to any but the simplest problems by traditional methods. However, now that large digital computers are generally available, a number of investigators are using them to adapt the essentially linear matrix structural analysis methods to these problems by various iterative and step by step procedures.

One way of formulating the problem is by means of the standard influence coefficient approach. The basic equation employed is as follows:

$$\sigma_u = \Gamma_{um} P_m + \Gamma_{uv} \epsilon_v \qquad (1)$$

In Equation 1, the σ_u's are the ordinary stress components at the various node points of the structure. An element of Γ_{um} gives the u^{th} stress in the linear redundant structure due to a unit m^{th} applied load, and P_m represents the actual applied loads. Also, an element of Γ_{uv} gives the u^{th} stress component in the linear redundant structure due to a unit initial strain at the v^{th} stress location in the unloaded, statically determinate structure. Finally, an element of ϵ_v represents the actual initial strain at the v^{th} stress location. One of the first applications of Equation 1 has been to thermal stress problems; more recently it has been useful in solutions involving nonlinear strains due to large deflections.

In the present case, the problem reduces in essence to a determination of what plastic strains to use for the initial strains ϵ_v in Equation 1. For a structure in a load-temperature-time environment, this task can be rather formidable, as the ϵ_v's are now functions of local temperature and time, as well as of local stress levels and their previous histories.

This paper examines one of the currently available step by step procedures for handling the foregoing problem, References 1 and 2. This is done at first only for the case of increasing loading, with the deformations being both time and temperature independent, and for uniaxial stress conditions. The preliminary objective is to present the method in the simplest way possible, consistent with a clear exposition of the basic ideas. A singly redundant truss is used as an example for this purpose. By this means it is also shown that the simplest and most obvious version of this step by step procedure is useful only in a limited way because of an early oscillatory divergence. The alternative version presented in References 1 and 2 does not have this disadvantage.

The paper next reviews, by making use of the Von Mises yield condition and the Prandtl-Reuss flow relations, the method of References 1 and 2 covers structures subject to biaxial plastic stress, and yields solutions corresponding to the flow theory of plasticity. By this approach, elastic strain recovery is permitted, but not the case of completely reversed loading. The technique is demonstrated by applying it to a 2024-T4 aluminum alloy shear lag structure which has been tested previously for the Air Force, Reference 9. The influence of the calculation step size is shown at this point, and it is observed that the calculated effective stress-strain relationship at key node points provides the clue to a satisfactory step size selection.

It is next shown how a very simple variation of the calculation procedure leads to a deformation theory solution. The result for the shear lag structure agrees very well with the corresponding flow theory solution.

Finally, the theory is extended as in References 1 and 2 to include primary creep, accumulated according to the strain hardening rule. The predictions of the procedure are compared with test data for an 1100-F aluminum shear lag structure as reported in Reference 9, and the agreement is surprisingly good.

It should be noted that the referenced tests were conducted on virgin material for continually increasing applied loads up to failure. Thus such difficult questions as cyclic loading and the accompanying Bauschinger effect are avoided; indeed, at present, there is apparently no workable method available for accommodating them. Nevertheless, a satisfactory method for predicting the behavior of structures being loaded into the plastic range for the first time will have many applications and it is to this question that the present effort is directed.

PLASTICITY ANALYSIS - UNIAXIAL CASE

Example Problem

The structure chosen for an example problem is the singly redundant pin-jointed truss shown in Figure 1. The exact results for the deformation and stresses in this truss, for nonlinear material properties, are easily obtained by direct numerical solution of the equations, and hence will be used without development.

The first step, in applying the finite element method, is to obtain the influence coefficient matrices Γ_{um} and Γ_{uv} for the linear, redundant structure. This requires specification of the geometry of the structure and the (linear) material properties of the individual structural elements. The geometry of the example truss problem is given in Figure 1. The only material

property required is Young's modulus, which is taken to be 10^7 psi for all members. In this case, we find

$$\Gamma_{um} = \begin{bmatrix} 0.207 \\ -0.293 \\ 0.707 \end{bmatrix}, \quad \Gamma_{uv} = 10^7 \begin{bmatrix} -0.414 & 0.207 & 0.207 \\ 0.586 & -0.293 & -0.293 \\ 0.586 & -0.293 & -0.293 \end{bmatrix}$$

for the case of the single applied load P.

The nonlinear time-independent plastic strains will be assumed to be given by a piece-wise linear approximation of the Ramberg-Osgood stress-strain relation; the latter may be written

$$\mathcal{E} = \frac{\sigma}{E} + \epsilon$$

where ϵ denotes the inelastic (or plastic) strains and is given by

$$\epsilon = \frac{3}{7}\left(\frac{\sigma}{\sigma_0}\right)^{\theta-1}$$

and where

$\mathcal{E}$ = total strain

σ = member stress

E = Young's modulus

σ_0 = reference stress (stress at secant modulus of 0.7E)

θ = nonlinear parameter

The material in the example truss problem is assumed to be an aluminum alloy with the following constants

$$E = 10^7 \text{ psi}, \quad \sigma_0 = 10^5 \text{ psi}, \quad \theta = 10$$

The approximate stress-strain curve actually used matches the Ramberg-Osgood values at 2000 psi stress intervals.

Step-by-Step Methods

The Bell Aerosystems Company, in References 1 and 2, presents what appears to be the simplest possible approach to this problem from a computational standpoint.* They merely perform a non-iterative step-by-step calculation in which all quantities including the inelastic strains ϵ_v are incremented periodically and then assumed to remain constant in the ensuing load intervals. The inherent difficulty in this approach is to establish the connection between successive steps. Two methods are suggested for doing this, both of which involve the strain

* While the methods designated here as Bell methods represent an early attempt to carry out inelastic analyses of structures, it must be acknowledged that these methods make use of devices previously used by others to solve inelastic problems. As one example, S.S. Mansom at the Lewis Research Laboratory, NASA, Cleveland, Ohio, had previously carried out inelastic analyses of turbine discs involving somewhat similar techniques.

increment from the prior step to predict quantities in the current step. The motivation is intuitive, with the notion that making the intervals sufficiently small is all that is necessary to achieve any desired degree of accuracy.

In order to explain the central ideas in the simplest possible terms, as indicated in the introduction, the development herein is discussed only in the detail necessary to analyze a redundant truss being loaded for the first time, and at room temperature. Generalization to biaxial plasticity and creep phenomena are discussed in the succeeding sections.

The step-by-step process for solving the problem is introduced by rewriting Equation 1 in the form

$$\sigma_u^{(k)} = \Gamma_{um} P_m + \Gamma_{uv} \epsilon_v^{(k-1)} \qquad (2)$$

where k is the cycle designation. This can be regarded as the fundamental equation for the non-iterative, step-by-step methods. The idea in formulating this equation, clearly, is that the inelastic strains of the previous cycle can be used to approximate the inelastic strains of the current cycle. It turns out, however, that the strains of the previous cycle may be incorporated in several ways, two of which constitute the Bell constant stress and the Bell constant strain methods of analysis. These two methods will now be described separately.

a. Bell Constant Stress Method

As indicated previously, in the step by step process to be considered here, one enters the k^{th} cycle with applied loads $P_m^{(k)}$ and initial strains $\epsilon_v^{(k-1)}$, the latter evaluated during the preceding cycle. The first operation of the current cycle is to determine $\sigma_u^{(k)}$ from Equation 2 by direct substitution. The other operation consists of determining $\epsilon_v^{(k)}$ for use in the next cycle. The Bell constant stress method consists of doing this in the most obvious way possible, namely by reading from the given stress-strain curve the plastic strains $\epsilon_v^{(k)}$ corresponding to the $\sigma_u^{(k)}$'s. The reason for the name "constant stress" is thus apparent; the operation is indicated schematically in Figure 2.

The results of applying this method to the example truss problem are shown in Figure 4, where the stress in the vertical member (Bar #3) has been plotted versus load. These results display a striking defect of the method due to the development of a sudden and catastrophic divergence, whose onset depends upon step size. This dependence, is such that any attempt to improve accuracy by reducing step size only hastens the occurrence of divergence. An explanation of this behavior is given in Reference 7. Because of this defect, the constant stress method in this form must obviously be eliminated from consideration as an acceptable method for general use.

b. Bell Constant Strain Method

In accordance with the previous discussion, the constant strain method again requires that as the first operation in the current cycle, $\sigma_u^{(k)}$ be evaluated by direct substitution in Equation 2. Thereafter, one determines $\epsilon_v^{(k)}$ for use in the next cycle as follows. Referring to Figure 3, for each member, point A is determined with stress-strain coordinates $\sigma_u^{(k)}$ and $\sigma_u^{(k)}/E + \epsilon_v^{(k-1)}$. A relaxed stress $\sigma_u^{*(k)}$ is now calculated with the same total strain, corresponding to point B on the given stress-strain curve. Note that here the total strain, rather than stress, remains unchanged — hence the name "constant strain" method. The required initial strain $\epsilon_v^{(k)}$ is that corresponding to the relaxed stress, as indicated on Figure 3.

The results of applying the constant strain method to the truss problem, for the three step sizes 5000, 500 and 50 pounds, are shown in Figure 5. The accuracy, for a given step size

is markedly inferior to that of the constant stress method, but the analysis is now free of any instability. The constant strain method is therefore selected for further use herein. More will be said about the step size and how to monitor it in the next section.

PLASTICITY ANALYSIS-BIAXIAL CASE

Review of Theory

Having presented the basic notations of the step by step procedure by means of a simple truss example, we proceed now to the case of more practical interest, that of a biaxially stressed structure. Essentially, the new procedure is identical to the one already developed with one exception; because of the biaxial stress we can no longer work directly from the stress-strain curve to obtain the plastic strains for use in Equation 2. Instead, we must employ the well-known concept of an "effective" stress-strain relationship in conjunction with the Von Mises yield criterion and the Prandtl-Reuss flow relations.

Using this approach, the effective stress-strain curve, when modified to include elastic strains ($\bar{\sigma}/E$) as well, is identical to the uniaxial stress-strain curve, say one obtained in a typical tension test. The standard procedure requires that, having calculated the ordinary stresses $\sigma_u^{(k)}$ for the k^{th} load level, we re-identify these stresses by means of a new subscript N, as follows:

$$\begin{bmatrix} \vdots \\ \sigma_u^{(k)} \\ \vdots \end{bmatrix} = \begin{bmatrix} \vdots \\ \sigma_{3N-2}^{(k)} \\ \sigma_{3N-1}^{(k)} \\ \sigma_{3N}^{(k)} \\ \vdots \end{bmatrix} \tag{3}$$

The stresses are now arranged in groups of three components at each node point N (two normal and one shear component). We now calculate the corresponding effective stresses $\bar{\sigma}_N^{(k)}$ for each of the nodes from the Von Mises formula

$$\bar{\sigma}_N^{(k)} = \left[\left(\sigma_{3N-2}^{(k)} \right)^2 - \left(\sigma_{3N-2}^{(k)} \right)\left(\sigma_{3N-1}^{(k)} \right) + \left(\sigma_{3N-1}^{(k)} \right)^2 + 3\left(\sigma_{3N}^{(k)} \right)^2 \right]^{\frac{1}{2}} \tag{4}$$

Note that by this definition, $\bar{\sigma}_N^{(k)}$ must be positive.

We now go to the tensile stress-strain curve for the material of interest (which is also the $\bar{\sigma}/E + \bar{\epsilon}(p)$ curve) and, using the Bell constant strain method, read from it the corresponding effective plastic strain $\bar{\epsilon}(p)_N^{(k)}$. This operation is identical to that previously described for the uniaxial case.

In accordance with the flow theory of plasticity, the increment in the effective strain $\Delta\bar{\epsilon}(p)_N^{(k)}$ over that of the preceding interval must be calculated next. This will be either positive or zero, depending upon whether or not elastic unloading is taking place. Thus,

$$\Delta \bar{\epsilon}(p)_N^{(k)} = \bar{\epsilon}(p)_N^{(k)} - \bar{\epsilon}(p)_N^{(k-1)} \qquad \left\{ \bar{\sigma}_N^{(k)} \text{ greater than any previous } \bar{\sigma}_N \right.$$

$$= 0 \qquad \left\{ \bar{\sigma}_N^{(k)} \text{ smaller than a previous } \bar{\sigma}_N \right. \tag{5}$$

The increments in the ordinary plastic strain components may now be obtained using the Prandtl-Reuss assumption together with the Von Mises yield condition.

$$\Delta \epsilon(p)_{3N-2}^{(k)} = \frac{\Delta \bar{\epsilon}(p)_N^{(k)}}{\bar{\sigma}_N^{(k)}} \left[\sigma_{3N-2}^{(k)} - \frac{1}{2} \sigma_{3N-1}^{(k)} \right]$$

$$\Delta \epsilon(p)_{3N-1}^{(k)} = \frac{\Delta \bar{\epsilon}(p)_N^{(k)}}{\bar{\sigma}_N^{(k)}} \left[\sigma_{3N-1}^{(k)} - \frac{1}{2} \sigma_{3N-2}^{(k)} \right] \tag{6}$$

$$\Delta \epsilon(p)_{3N}^{(k)} = \frac{\Delta \bar{\epsilon}(p)_N^{(k)}}{\bar{\sigma}_N^{(k)}} \left[3\sigma_{3N}^{(k)} \right]$$

The total, ordinary plastic strain components are obtained by addition,

$$\begin{bmatrix} \vdots \\ \epsilon(p)_{3N-2}^{(k)} \\ \epsilon(p)_{3N-1}^{(k)} \\ \epsilon(p)_{3N}^{(k)} \\ \vdots \end{bmatrix} = \begin{bmatrix} \vdots \\ \epsilon(p)_{3N-2}^{(k)} \\ \epsilon(p)_{3N-1}^{(k-1)} \\ \epsilon(p)_{3N}^{(k-1)} \\ \vdots \end{bmatrix} + \begin{bmatrix} \vdots \\ \Delta\epsilon(p)_{3N-2}^{(k)} \\ \Delta\epsilon(p)_{3N-1}^{(k)} \\ \Delta\epsilon(p)_{3N}^{(k)} \\ \vdots \end{bmatrix} \tag{7}$$

These components together with the new applied loads $P_m^{(k+1)}$ may be substituted in Equation 2 to obtain $\sigma_u^{(k+1)}$, in the next load cycle.

Determination of Calculation Step Size

It should be noted that, according to the Bell constant strain method, every predicted value for $\bar{\epsilon}(p)_N^{(k)}$ together with its accompanying value $\bar{\sigma}_N^{(k)}$ constitutes an approximation to a point on the actual effective stress-strain curve. The excellence of the approximation is directly related to the loading increment; this can be inferred from the truss results given previously. Thus it is only necessary to monitor this agreement for one or more of the

critically loaded nodes to determine whether the step size is satisfactory. This will be illustrated in connection with the shear lag structure investigation, which follows.

Description of Shear Lag Structure

Several very useful tests have been performed for the Air Force upon shear lag structures, Reference 9. The specimens are integrally stiffened as shown in Figure 6 and are made of 2024-T4 aluminum alloy in the case of the room temperature, time independent tests to be considered here.

Material properties in the form of tension test data are presented in Figure 8. Considerable anisotropy exists, as indicated by the disparity between the longitudinal and transverse properties, the latter being in the loading direction of the structure. A piece-wise linear, approximate curve has been selected to represent the material; as shown in Figure 8 it is designated RO2M and has been chosen to match the data in the y direction of the shear lag specimen. Note also that the maximum strains recorded are of the order of 0.01, whereas the maximum strains recorded in the shear lag tests are around 0.02. Thus there is some doubt as to whether the idealized curve correctly represents the test material properly in this high strain region. The Young's modulus is taken as $E = 10.2 \times 10^6$ psi.

The locations of the strain gages for the test of the stiffened plate are shown in Figure 10. The plate was loaded by applying tension to the stiffener in steps of 1000 to 6000 pounds, gage readings being taken at each step. It was unloaded in steps of 1500 pounds to zero, and finally progressively loaded to failure. Buckling occurred at a load of 23,000 pounds and fracture at 25,800 pounds. Data from this test appear in Figures 11 to 14.

Linear Analysis of Shear Lag Structure

The two influence coefficient matrices Γ_{um} and Γ_{uv} for the structure may be obtained conveniently by either the matrix force or direct stiffness method. It is merely necessary that they give conventional stress components at all of the nodes for both externally applied loads and initial strains, as discussed previously. In the present case, the force method has been used, with the idealized structure consisting of the usual bars and shear panels located as shown in Figure 7. Only the upper right-hand quadrant need be considered, taking advantage of the structure's double symmetry. As idealized, there are sixty-four node points in all. Nodal stresses are averages of values occurring at each node.

Results of Flow Theory Shear Lag Structure Analysis

Before getting into a comparison of analysis and test results, let us look at a plot of the tensile stress-strain curve, RO2M, and how it compares with the predicted effective stress-strain relationship. Such a comparison is found in Figure 9 for the node corresponding to the center of the specimen, which is the point of highest strain throughout the structure. It can be seen there that for a step size of $\Delta P = 500$ lb., the agreement is rather poor. For $\Delta P = 50$ lb. the agreement is much better, while for $\Delta P = 5$ lb., the predicted values fall right on the proper curve. The 7094 computer time for this best result and a maximum load of $P = 16{,}760$ lb is approximately 20 minutes.

Going now to the predicted strain distributions, which are shown in Figures 11 to 14, together with the corresponding test values, along the two strain-gage lines. In these plots the calculated results are linearly interpolated values between node points. The first figure gives elastic results; the agreement in all cases is seen to be rather good, giving the necessary confidence in the accuracy of the basic influence coefficient matrices. It is observed also that the specimen achieves its basic purpose reasonably well of displaying a pronounced shear lag effect, with the highest strains in both directions occurring at the central node, as expected.

As the applied load increases through 7070 lbs, the strains at the central node become plastic. During the tests, the strain gages here continued to function through an applied load level of 14,600 pounds; beyond this point the x gage failed to record. The y gage failed also above a load level of 16,760 pounds, and consequently this is the highest level considered in the comparison of test and analysis, even though the plate did not buckle until P = 23,000 pounds.

The proportional limit for the test specimen material occurs at a strain of approximately 0.004 in./in., as shown on Figure 8. Bearing this in mind and examining Figures 11 to 14, it is seen that plastic behavior is primarily confined to a fairly small region around the central node, and we thus have a case of contained plasticity. The analysis predicts a very pronounced strain redistribution extending somewhat beyond this region. This is indicated by a comparison of the plastic results with extrapolated elastic results shown as dotted curves on Figure 14.

As for agreement with test values, the analysis now substantially under-predicts the strain gage readings where plasticity is most pronounced. Since the elastic results agree so much better, one must assume that the difficulty lies somewhere in the plasticity part of the correlation. It was mentioned previously that the idealization of the stress-strain curve RO2M of Figure 8 was open to question at the high strain end because of the absence of test points. Accordingly, an additional run was made for a revised curve extending horizontally beyond the last indicated test point. The plastic strains at the critical central node are increased approximately 10 percent by so doing. This represents an appreciable closing of the gap, but the gap nevertheless remains.

The question of anisotroppy of the 2024-T4 material also naturally arises. While only preliminary calculations taking this into account have been made so far, it is felt that this effect cannot further improve the agreement. It will have the beneficial effect, however, of making the agreement more consistent as between the x and y directions.

Deformation Theory Analysis

Solutions by the deformation theory of plasticity have traditionally been considered to be more easily obtainable than flow theory solutions. This is, of course, because only the stresses at the final applied load level need be considered, rather than the stress histories developed during loading. It is, therefore, of interest to determine whether similar benefits are attainable in the case of the finite element analyses currently being considered.

Once again, a solution of Equation 1 is required, this time, such that the initial strains ϵ_0 satisfy the deformation theory of plasticity. This can be accomplished as follows. Equation 2, the "k^{th} cycle" stress equation of the preceding section can be used intact if it is understood that $P_m^{(k)}$ is the peak load at which the results are required and does not change from one cycle to another as before. The solution is therefore iterative.

The intra-cycle procedure employed for the determination of the equivalent strain for the k^{th} cycle is the same as before, namely the constant strain method. At this point, however,

the equivalent strain itself, not its increment, is resolved into the node plastic strains by utilizing an adaptation of the Prandtl-Reuss equations, thus:

$$\epsilon(p)^{(k)}_{3N-2} = \frac{\bar{\epsilon}(p)^{(k)}_N}{\bar{\sigma}^{(k)}_N}\left[\sigma^{(k)}_{3N-2} - \frac{1}{2}\sigma^{(k)}_{3N-1}\right]$$

$$\epsilon(p)^{(k)}_{3N-1} = \frac{\bar{\epsilon}(p)^{(k)}_N}{\bar{\sigma}^{(k)}_N}\left[\sigma^{(k)}_{3N-1} - \frac{1}{2}\sigma^{(k)}_{3N-2}\right] \qquad (8)$$

$$\epsilon(p)^{(k)}_{3N} = \frac{\bar{\epsilon}(p)^{(k)}_N}{\bar{\sigma}^{(k)}_N}\left[3\sigma^{(k)}_{3N}\right]$$

These are now available for the stress equation of the next cycle.

Three analyses, one at P = 11,600 pounds, one at P = 14,600 pounds and one at P = 16,760 pounds were performed on the shear lag specimen by this deformation theory procedure. The results were practically identical with those shown in Figures 12 to 14. The convergence to each of these results was obtained after less than thirty cycles of iteration, when the solution stabilized. The machine time for each calculation was approximately four minutes.

In the case of solutions like this, where the two theories give practically identical results, the deformation theory approach is naturally very attractive because of the greatly reduced machine time. However, the question remains of determining when to expect the results to agree in this manner.

CREEP ANALYSIS-BIAXIAL CASE

Review of Theory

Strains due to creep constitute an additional form of initial strain, and can be handled in an analogous way to that already discussed for biaxial plasticity by the flow theory. It is only necessary to select a method for evaluating these time-dependent strains based upon the material properties and to add them to the plastic strains prior to insertion in the basic Equation 2.

A familiar relationship used to match the creep behavior in a tensile creep test performed at constant stress and constant temperature is

$$\epsilon(c) = \alpha t^{\gamma}\left(e^{\beta\sigma} - 1\right) \qquad (9)$$

in which $\epsilon(c)$ is the tensile creep strain, t is the elapsed time, σ is the constant tensile stress, and α, β, and γ are empirical constants for the particular test temperature.

The assumption is made that there exists an effective creep strain $\epsilon(c)$ in a biaxial situation which can be represented by Equation 9 by replacing tensile stress by the Von Mises effective stress. The further assumption is made that this effective creep strain can be resolved into nodal creep strains by use of the Prandtl-Reuss law.

We now desire to generalize to situations in which the stresses vary with time. One well-known procedure for doing this, the strain-hardening rule, has been determined to be most appropriate for the present purposes, and its use will be described presently in connection with the k^{th} calculation cycle.

One enters the k^{th} cycle with applied loads $P_m^{(k)}$, and with all the initial strains, plastic and creep, as calculated during the preceding cycle. The stresses $\sigma_u^{(k)}$ are calculated immediately using Equation 2, and the effective stresses $\bar{\sigma}_N^{(k)}$ are obtained from Equation 4. At this point the plastic strains to be employed in the next cycle are calculated identically as before.

The strain-hardening rule refers only to the routine for obtaining the effective creep strain increment at a node, and proceeds as follows. Referring to Figure 15, one goes to the constant effective stress-temperature curve $(\bar{\sigma}^k, T^k)$ relevant to the node and the cycle, and locates upon it the point with ordinate $\bar{\epsilon}(c)^{k-1}$. The corresponding abscissa, designated $t^{*(k)}$, is called the reference time and is generally different from the actual elapsed time at the start of the cycle. The required effective creep strain increment $\Delta\bar{\epsilon}(c)_N^k$ is that corresponding to the increase in time from t^{*k} to $(t^{*k} + \Delta t^k)$ as shown on Figure 15, Δt^k being the time increment. $\Delta\bar{\epsilon}(c)_N^k$ is substituted in the Prandtl-Reuss, Equation 6, together with the stresses indicated there. The creep initial strains are then obtained as in Equation 7.

Although thermal strains due to temperature gradients throughout the structure have not been specifically mentioned, if they are present they too may be added to the other initial strains at this point.

In summary, the steps in the k^{th} calculation take the following order

(1) Solution of Equation 2 for $\sigma_u^{(k)}$

(2) The calculation of effective stress according to Equation 4

(3) The determination of the node plastic strains

(4) The determination of the node creep strains

(5) The addition of the plastic and creep strains above to give the initial strains for the next cycle.

Description of Structure and Tests

The description of the shear lag structure to be analyzed in this section and tests for the material properties may be found in Reference 9. The shear lag structure was manufactured from 1100-F aluminum. It was of the same physical dimensions as the structure of Figure 6. The idealization of the upper right quadrant remains unchanged.

Material properties for the creep analysis were obtained from uniaxial strain-time tests for constant tensile stress. The temperature of these material properties tests was 206°C, identical to that of the structure test. The curves for these tests are presented in Figure 16 together with the fitted curves from Equation 9. The constants of the equation were obtained from Reference 9 and are as follows:

$$\alpha = 0.650 \times 10^{-4} \qquad \beta = 0.700 \times 10^{-3}\ in^2/lb$$

$$\gamma = 0.500$$

Ordinary tensile stress-strain tests were performed at room temperature on coupons cut from the x and y orientations of the plate material. The data and faired curve are presented in Figure 17. Tensile stress-strain data for 206°C are also plotted here. These data were obtained from the intersections of the test curves on the zero time axis in Figure 16. A piecewise linear representation TC1 was fitted to this latter data.

The location of the strain gages on the structure is given in Figure 18. The shear lag specimen was tested for a total of three hours at 206°C. An applied load of 1600 lbs. was applied at the start, and this was increased to 2020 lbs. at the end of the first hour. It was held constant thereafter until the end of the test.

Results of Creep Shear Lag Analysis

The predicted strain distributions along the x-axis and along the section x = 1 in. at t = 0.06 hr., t = 1.10 hr. and t = 3.00 hr. elapsed times, are given in Figures 19 to 21, together with the experimental data of Reference 9. Test data are not available for the y-node strains at the center node, and so this correlation point of critical significance does not exist.

The curve of Figure 22, effective stress versus strain at the central node, exhibits the shapes characteristic to the various regions of the load-time sequence. The initial linear segment represents elastic loading, followed by the region of negative curvature representing loading into the plastic range, all at assumed zero time. Thereafter, the applied load remains constant for one hour; during this time there is a stress redistribution in the structure due to creep. This particular node unloads, as evidenced by the reduction in effective stress, although the total strain is growing continuously. The applied load is now increased to 2020 lbs. Because of the previous elastic strain recovery, the effective stress at first goes up elastically, and then becomes plastic once more. Once the applied load reaches its final value, redistribution again takes place due to creep effects.

In the initial stages of creep the curve is very sensitive to time increment size and it is necessary to choose exceptionally small time increments in this region if good accuracy is to be achieved. The time increments employed are as shown in Figure 22.

Considering the simplicity of the expressions employed to describe as complex a phenomenon as creep and the liberal assumptions made in the process, the correlation between analysis and experiment, as evidenced by Figures 19 to 21, is surprisingly good.

REFERENCES

1. Padlog, J., Huff, R. D., and Holloway, F. G., Unelastic Behavior of Structures Subjected to Cyclic, Thermal and Mechanical Stressing Conditions, WADD TR-60-271, Wright Air Development Division, Wright-Patterson AFB, Ohio, December 1960.

2. Gallagher, R. H., Padlog, J., and Bijlaard, P. P., "Stress Analysis of Heated Complex Shapes," ARS Journal, Vol. 32, No. 5, pp. 700-707, May 1962.

3. Manson, S. S., "Thermal Stresses in Design," Machine Design, Parts 11, 12, and 13, 9 and 23 July, 6 August 1959.

4. Mendelson, A., and Manson, S. S., Practical Solutions of Plastic Deformation Problems in Elastic-Plastic Range, NACA TN 4088, September 1959.

5. Millenson, M. B., and Manson, S. S., Determination of Stresses in Gas Turbine Disks Subjected to Plastic Flow and Creep, NACA Report No. 906, 1948.

6. Denke, P. H., "Digital Analysis of Plasticity in Plates," Appendix C of Compressive Loads on Structural Fatigue at Elevated Temperatures, ASD-TDR-62-448, Aeronautical Systems Division, Wright-Patterson AFB, Ohio, October 1962.

7. Mentel, T. J. Comparison of Matrix Methods for Inelastic Structural Analysis, Grumman Advanced Development Report No. ADR 02-11-64.1, February 1964.

8. Mentel, T. J., On Evaluation of Matrix Methods for Nonlinear Biaxial Stress Analysis, Grumman Advanced Development Report No. ADR 02-11-64.2, June 1964.

9. Percy, J. H., Loden, W. A., and Navaratna, D., A Study of Matrix Analysis Methods for Inelastic Structures, RTD-TDR-63-4032, Research and Technology Division, Wright-Patterson AFB, Ohio, October 1963.

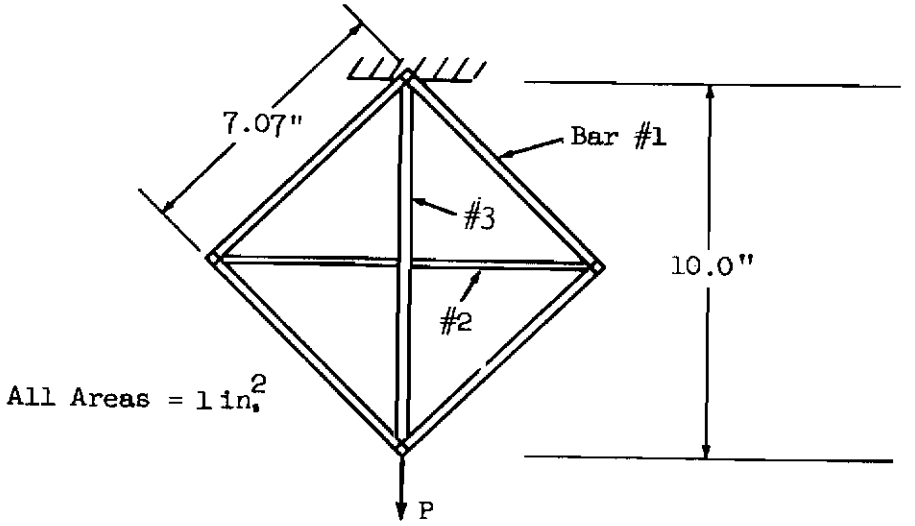

Figure 1. Truss Structure

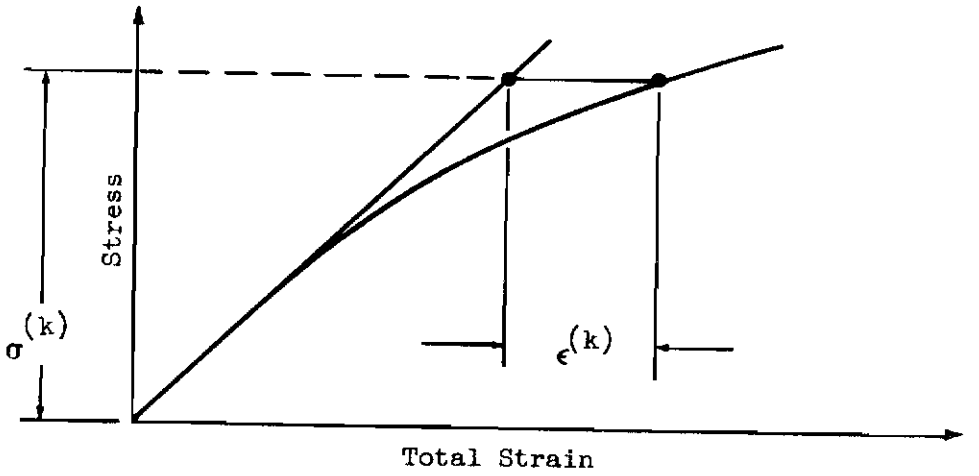

Figure 2. Bell Constant Stress Method

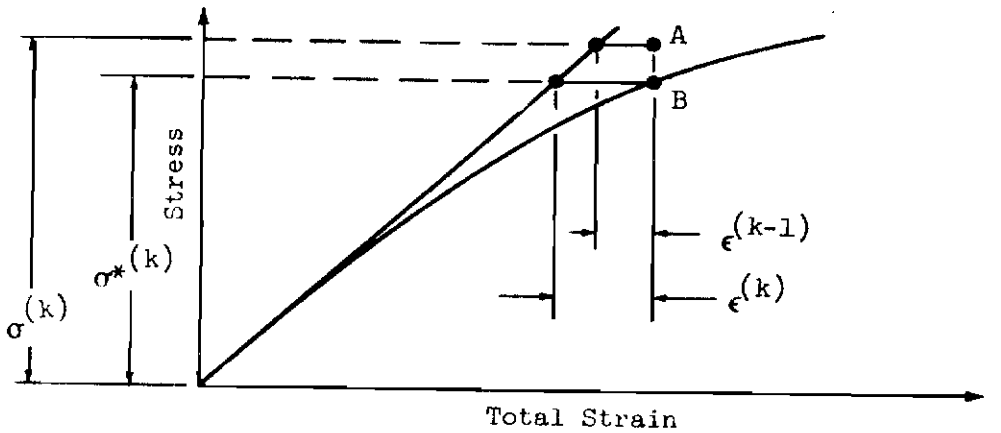

Figure 3. Bell Constant Strain Method

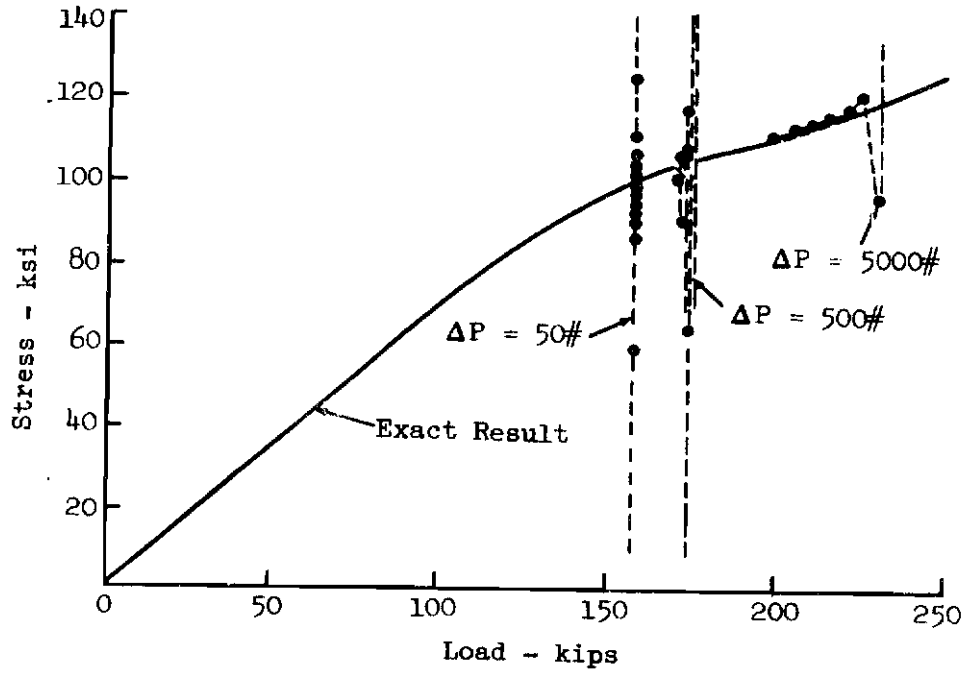

Figure 4. Results of Bell Constant Stress Method for Bar #3 of Truss

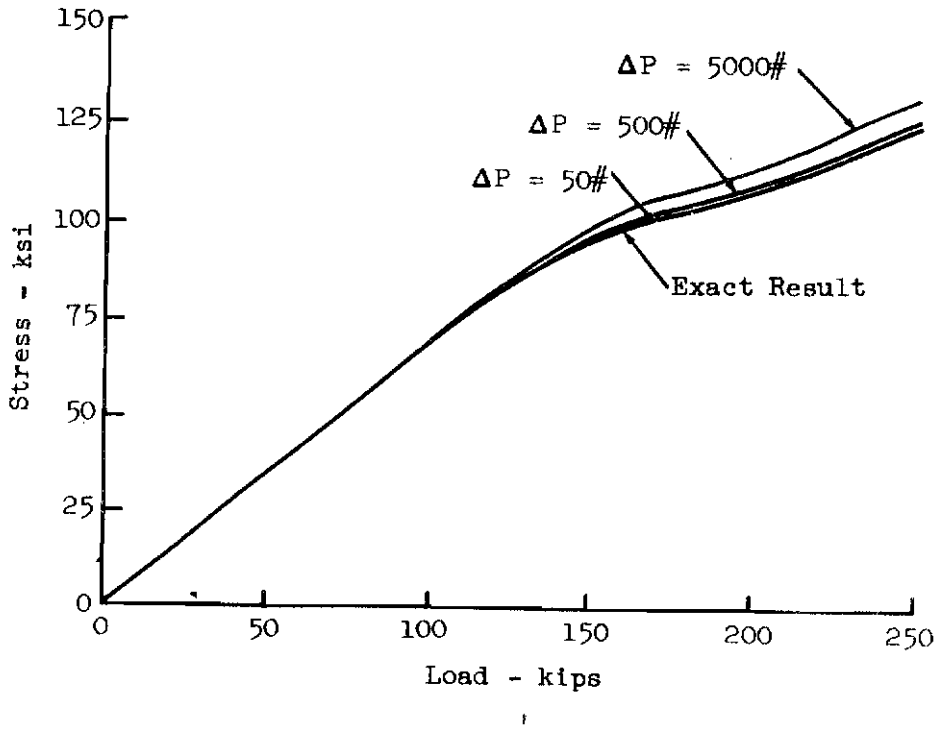

Figure 5. Results of Bell Constant Strain Method for Bar #3 of Truss

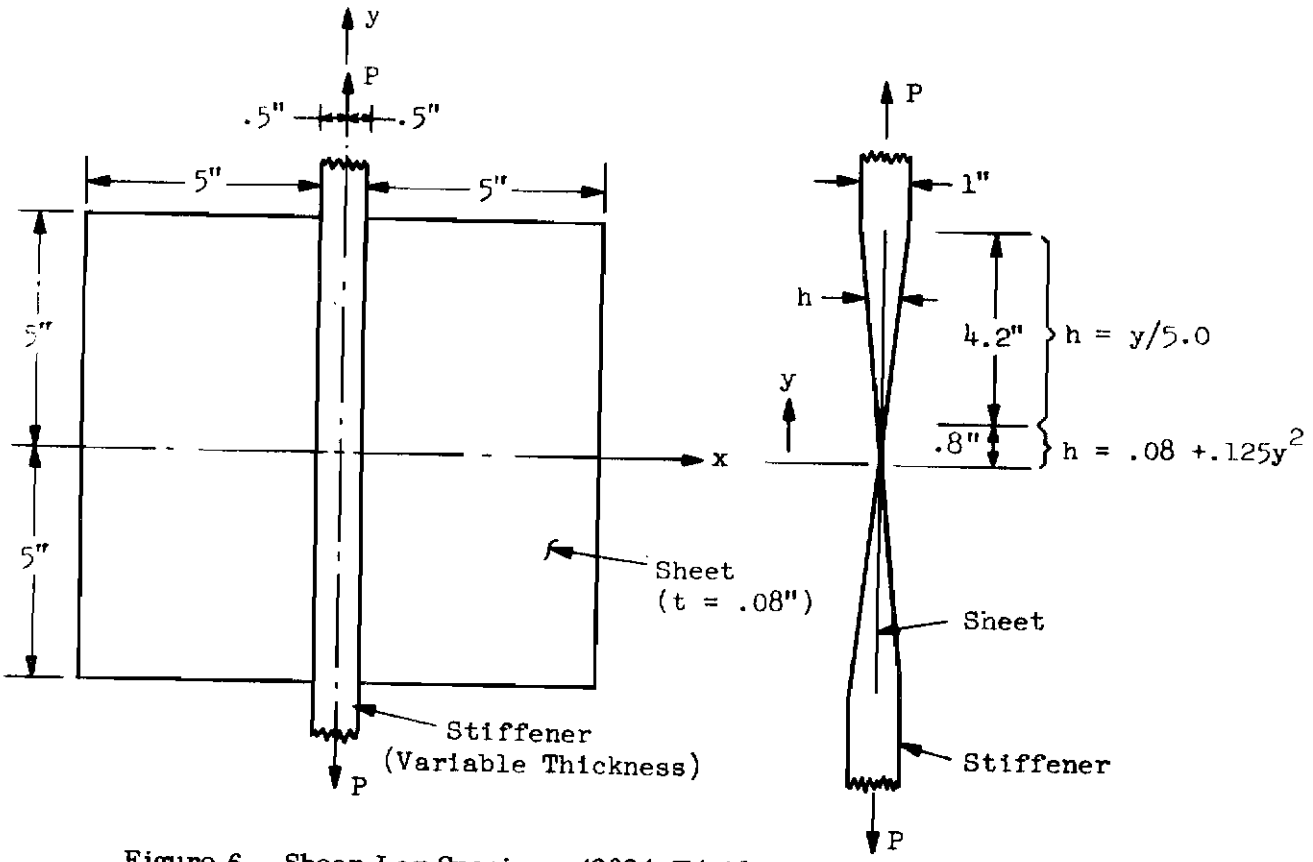

Figure 6. Shear Lag Specimen (2024-T4 Aluminum Alloy, Reference 9)

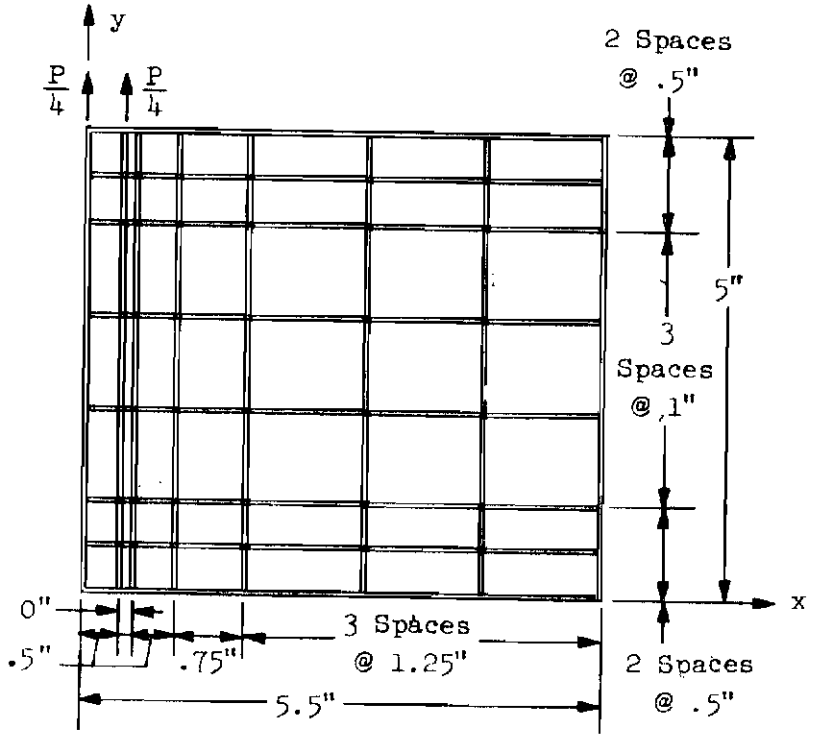

Figure 7. Idealized Upper Right Quadrant of Structure

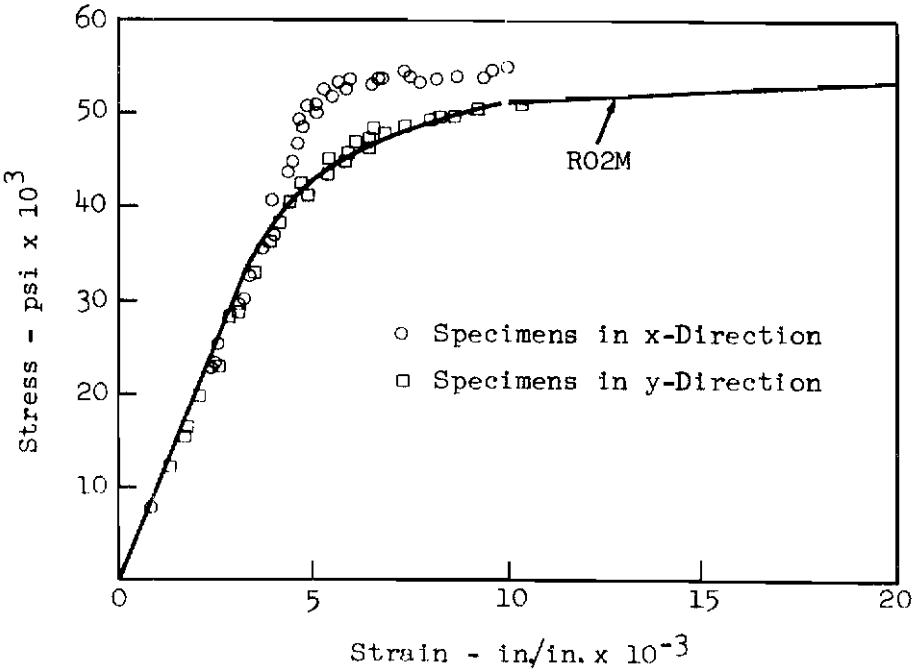

Figure 8. 2024-T4 Aluminum Alloy Stress-Strain Data and Curve RO2M

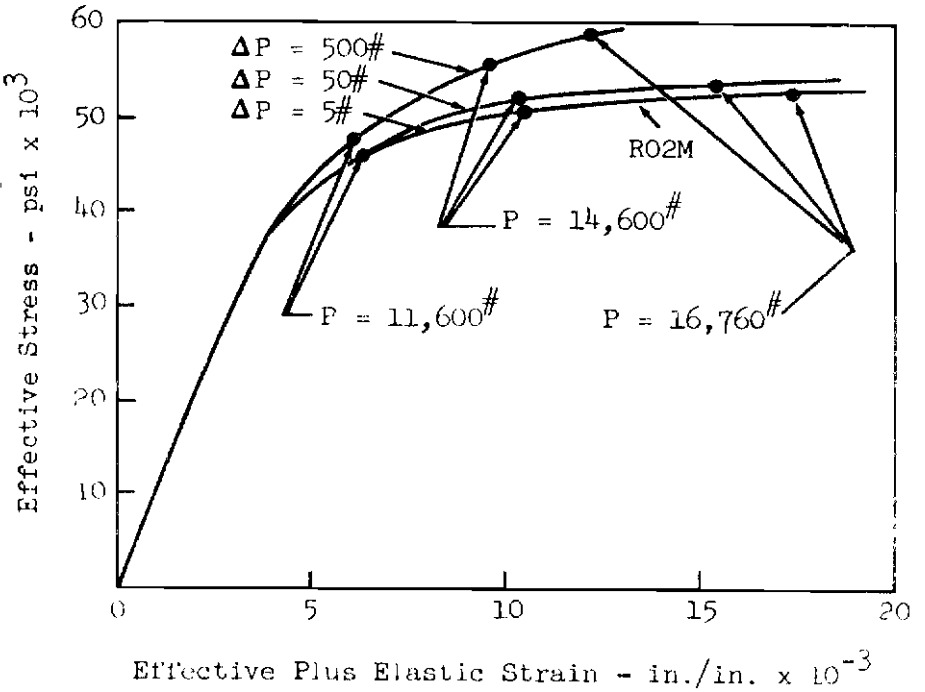

Figure 9. Comparison of Predicted Effective Stress - Strain Relationship with RO2M at (0, 0) for Various Load Increments

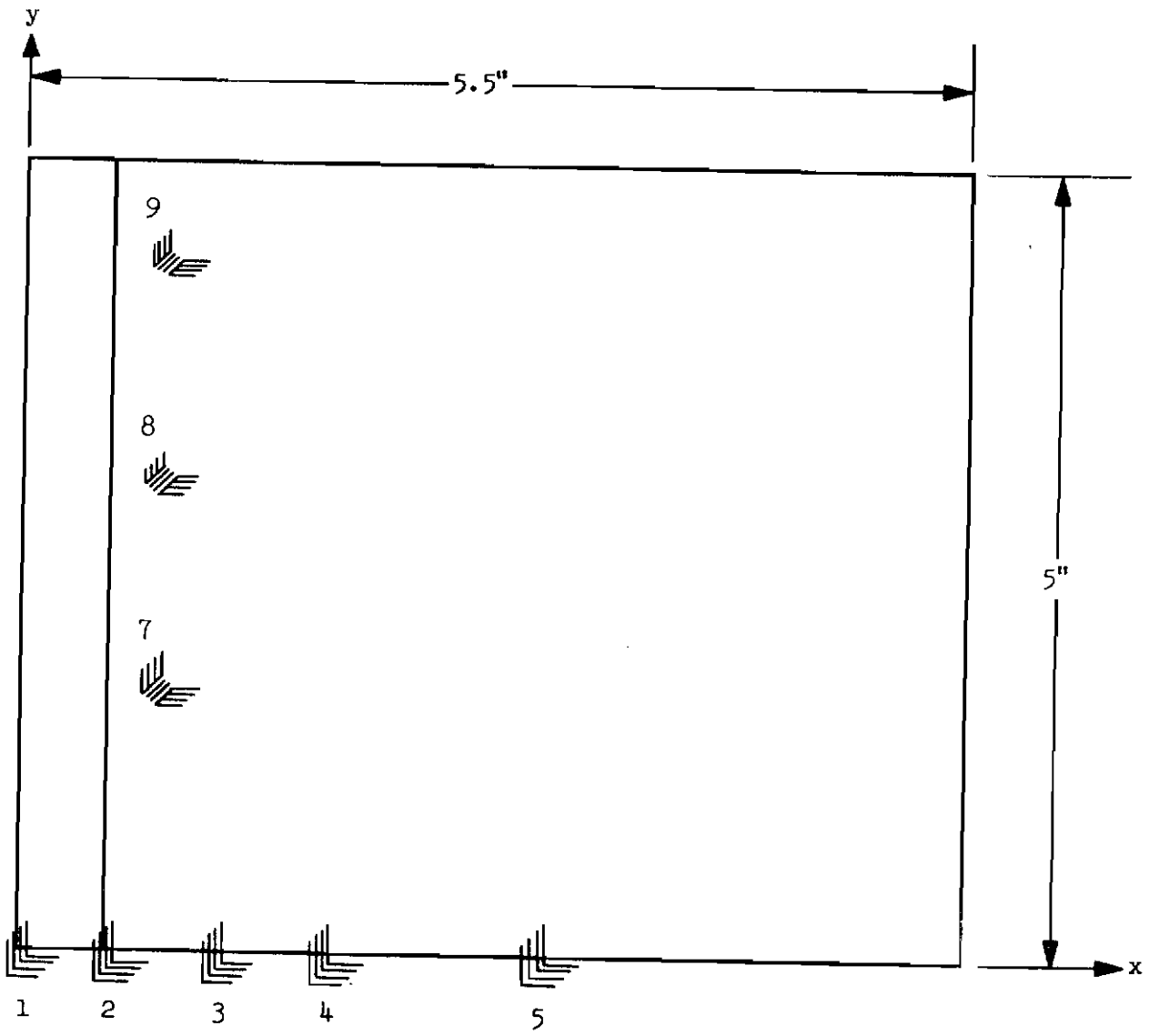

Gage Nos.		Co-ordinates		Gage Nos.		Co-ordinates	
Front	Back	x	y	Front	Back	x	y
1	11	0.0	0.0	6	16	-1.125	0.0
2	12	0.5	0.0	7	17	0.8125	1.5625
3	13	1.125	0.0	8	18	0.8125	2.8125
4	14	1.750	0.0	9	19	0.8125	4.0625
5	15	3.000	0.0				

Figure 10. Instrumentation of 2024-T4 Aluminum Alloy Specimen with Strain Gages (Reference 9)

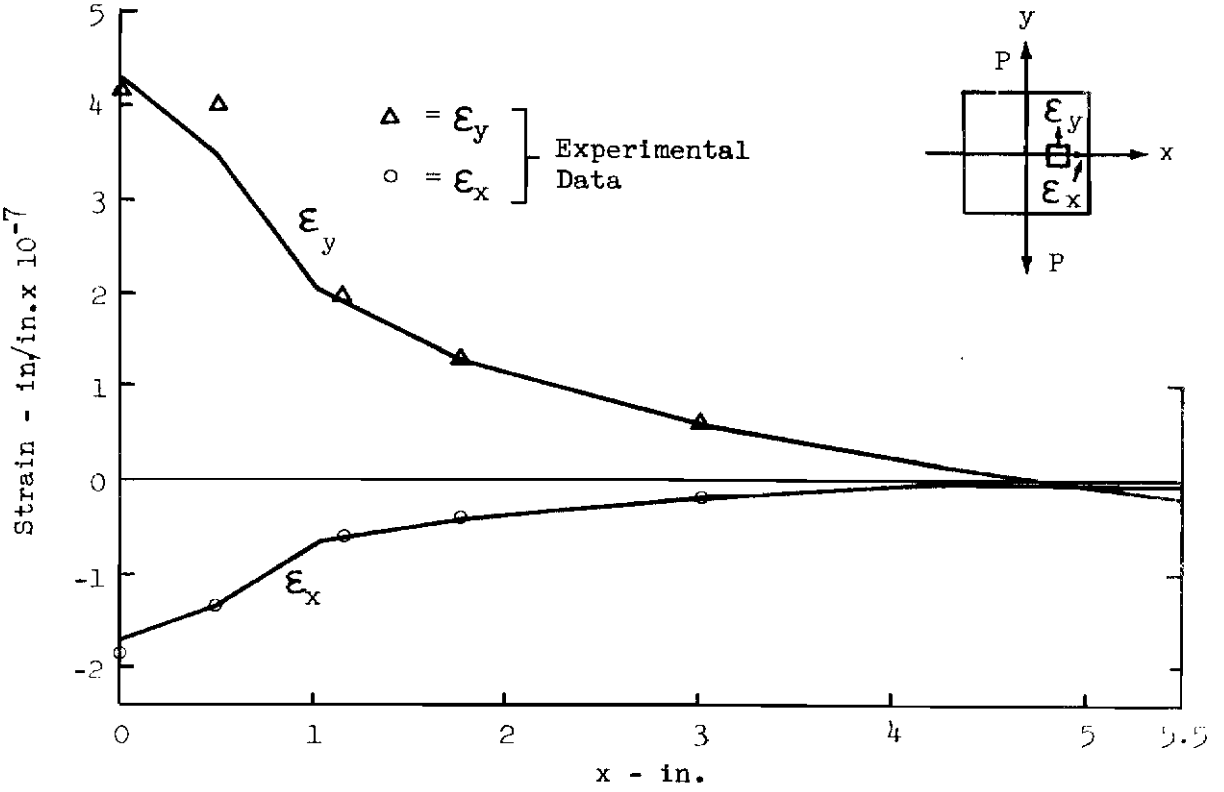

Figure 11a. Unit Strain Distribution on x - Axis for P = 1#

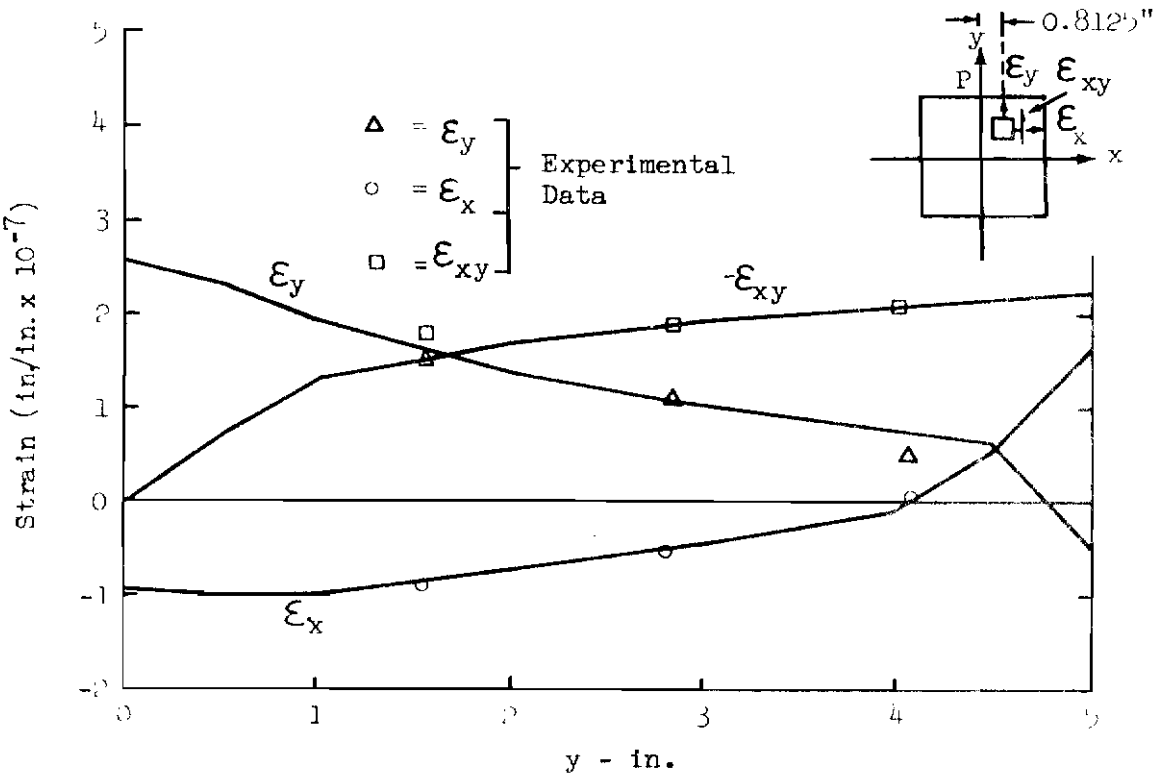

Figure 11b. Unit Strain Distribution on x = 0.8125 for P = 1#

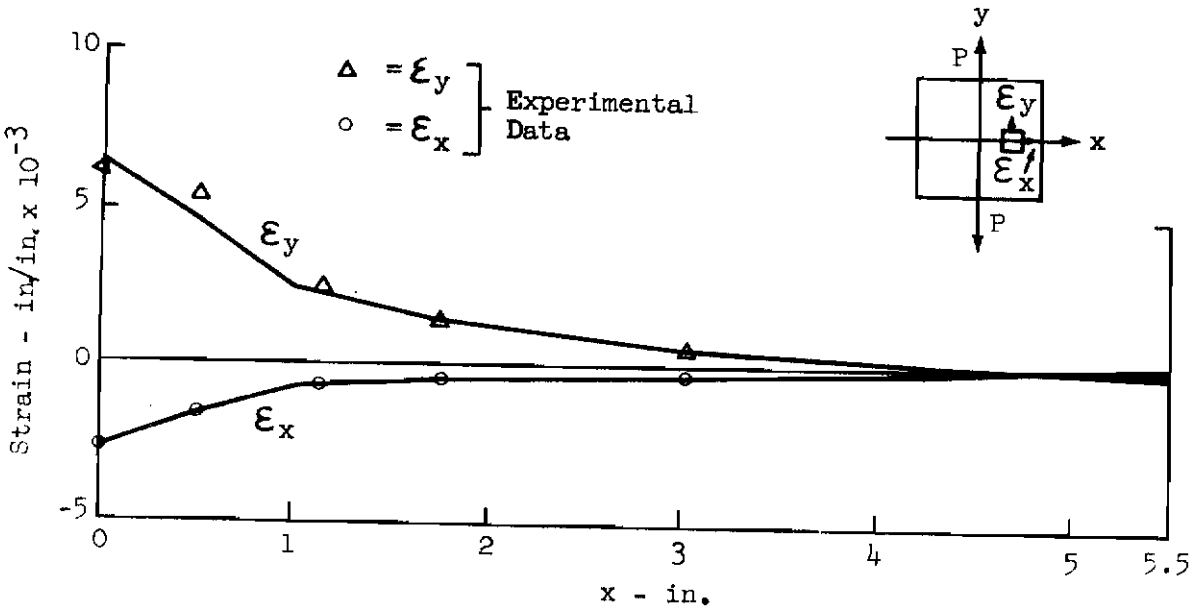

Figure 12a. Strain Distribution on x - Axis for P = 11,600 lbs. and ΔP = 5 lbs.

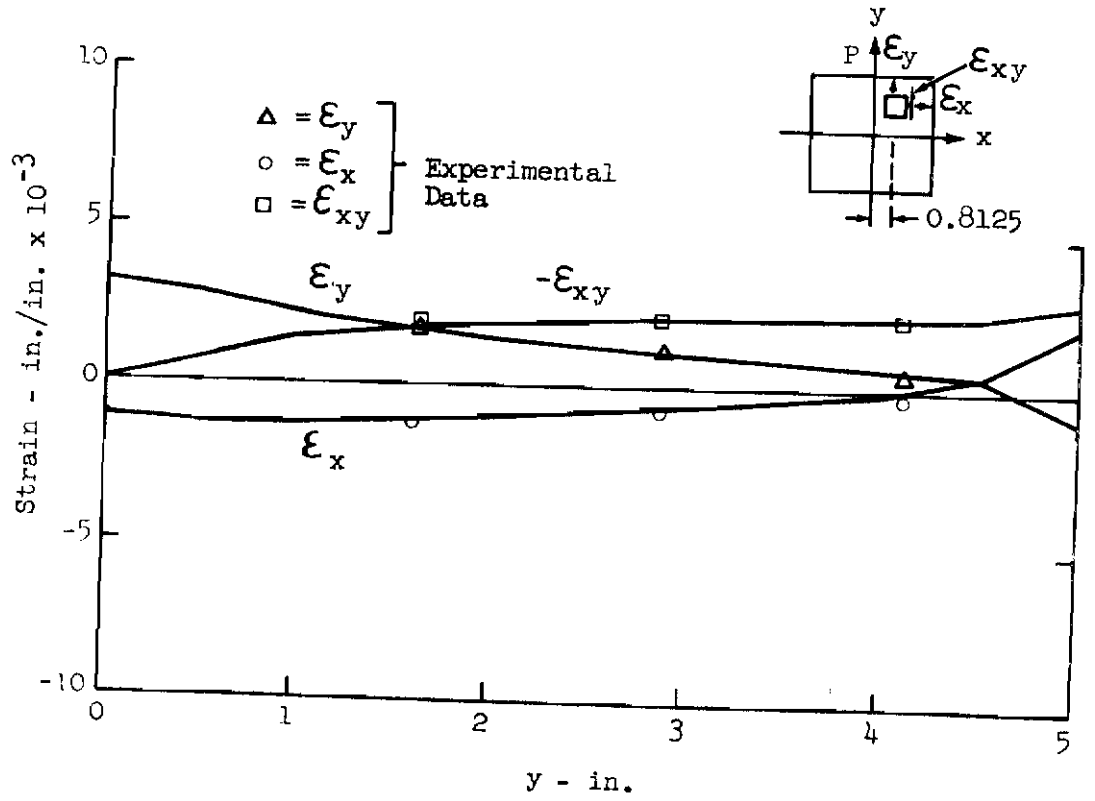

Figure 12b. Strain Distribution on x = 0.8125 for P = 11,600 lbs and ΔP = 5 lbs.

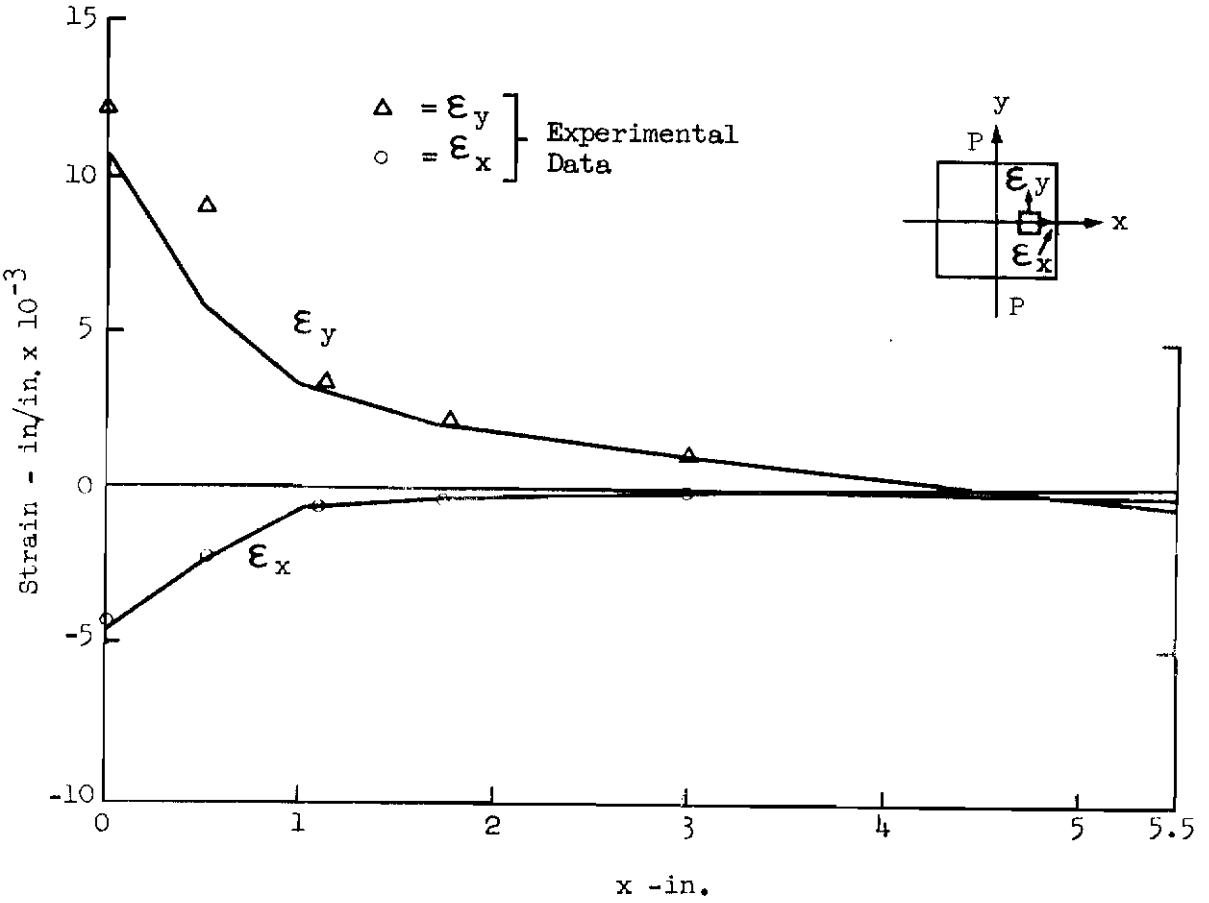

Figure 13a. Strain Distribution on x - Axis for P = 14,600# and ΔP = 5#

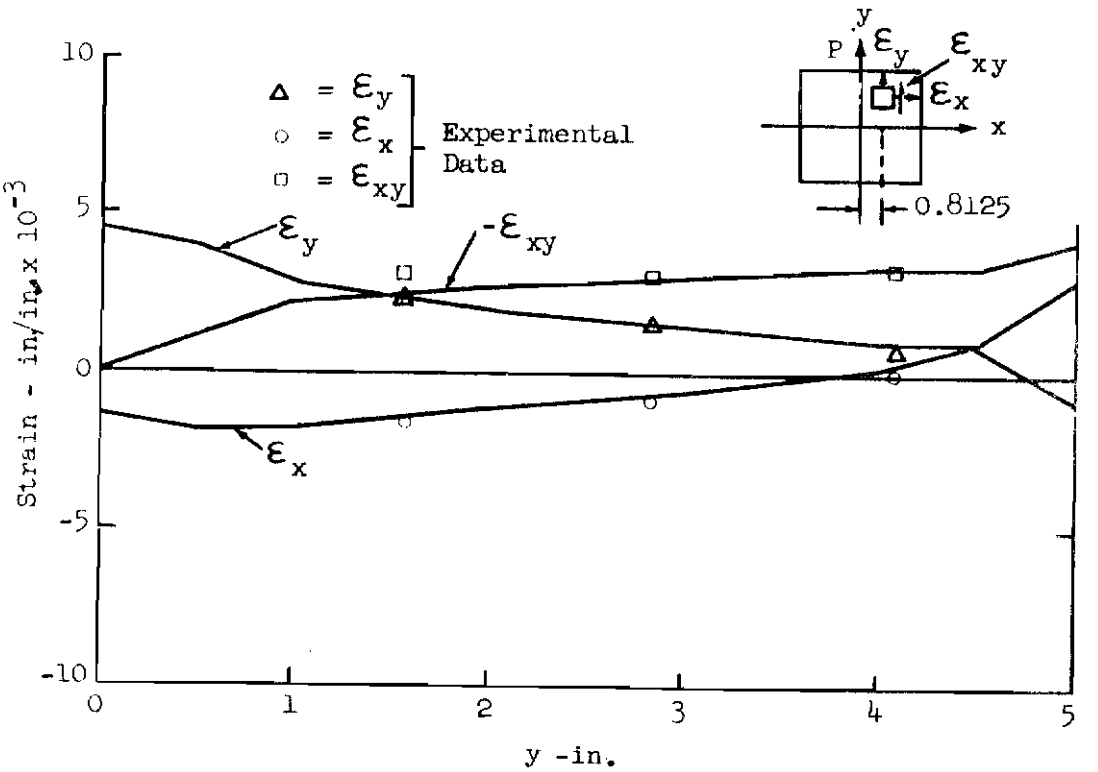

Figure 13b. Strain Distribution on x = 0.8125 for P = 14,600# and ΔP = 5#

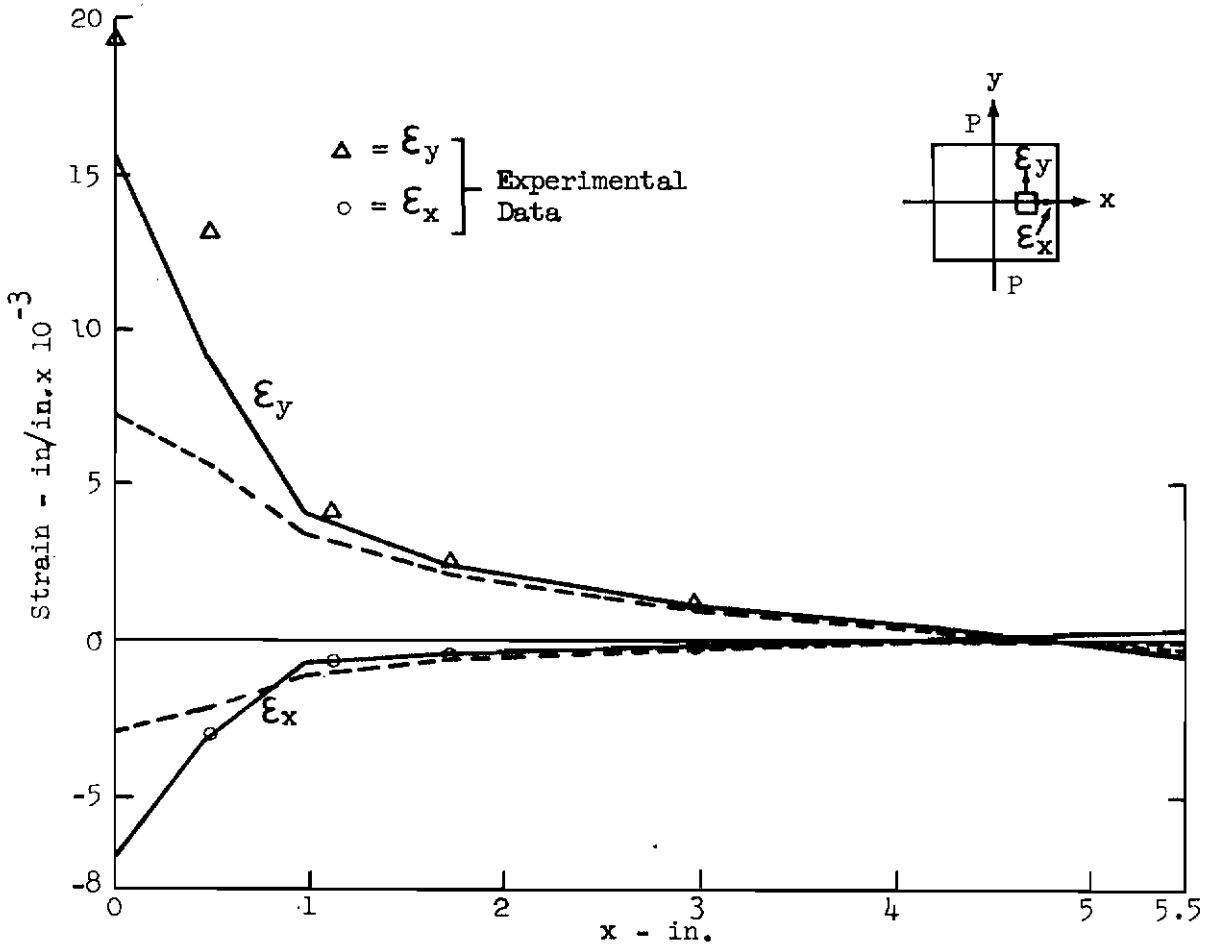

Figure 14a. Strain Distribution on x - Axis for P = 16,760 lbs., and ΔP = 5 lbs.

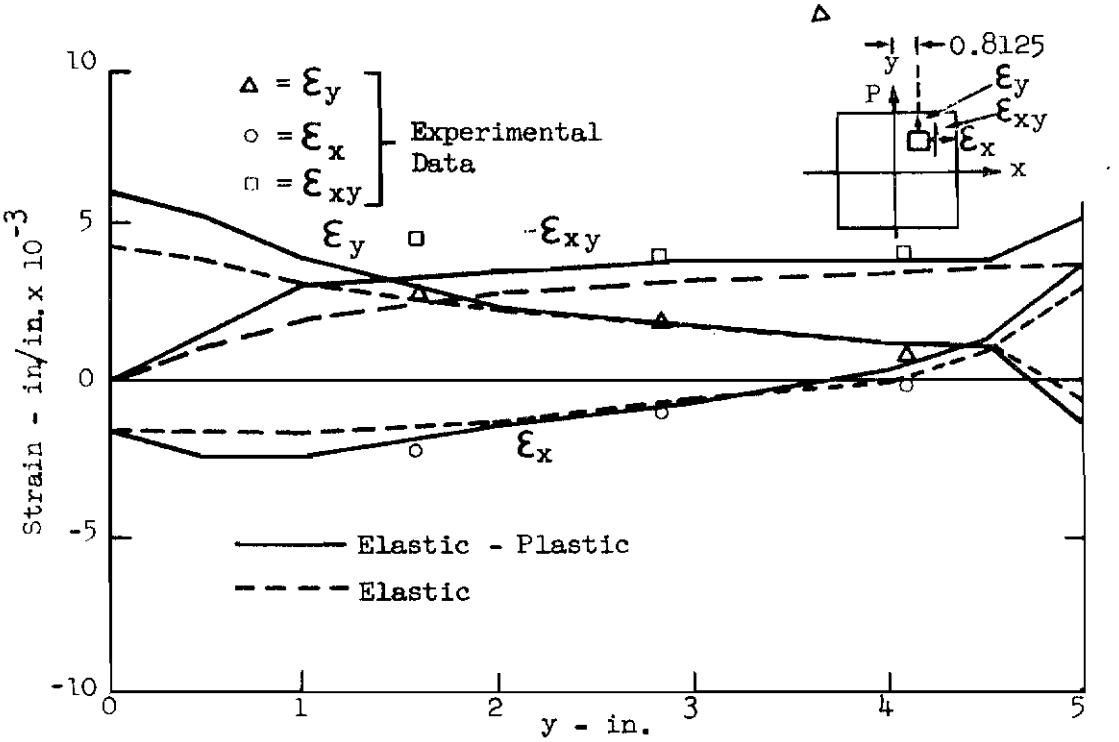

Figure 14b. Strain Distribution on x = 0.8125 in for P = 16,760 lbs. and ΔP = 5 lbs.

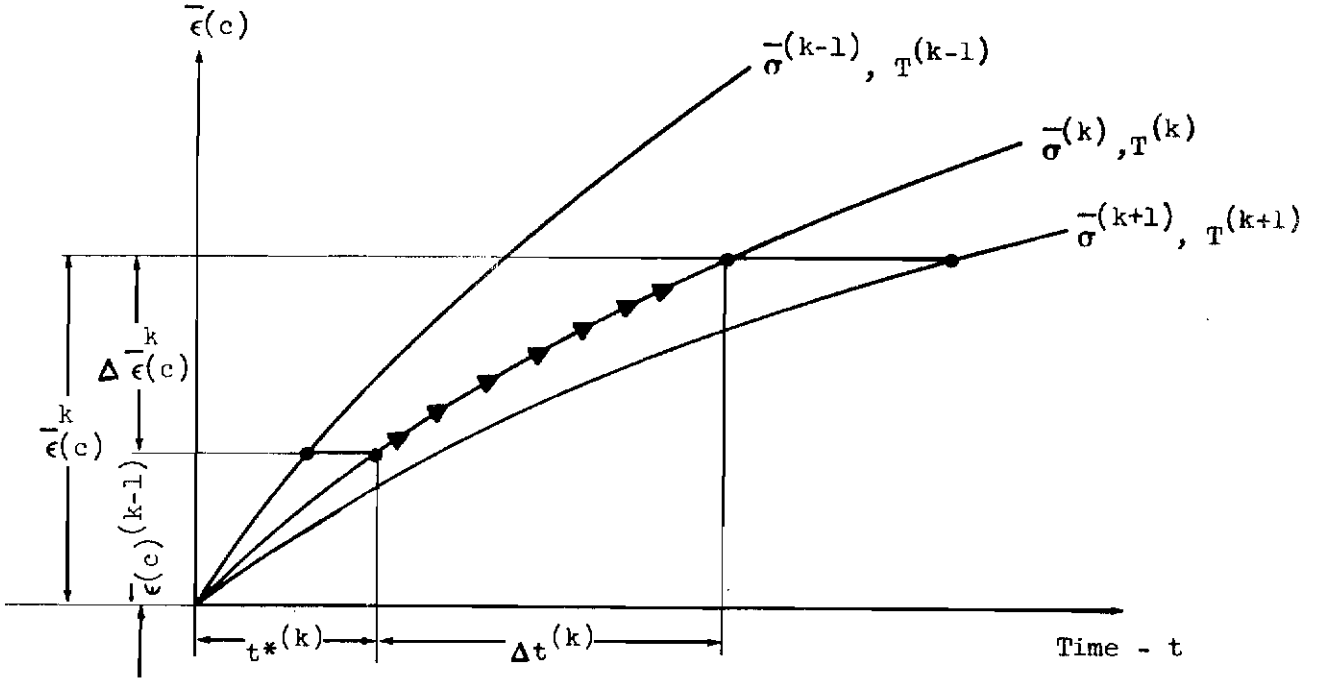

Figure 15. The Strain Hardening Rule

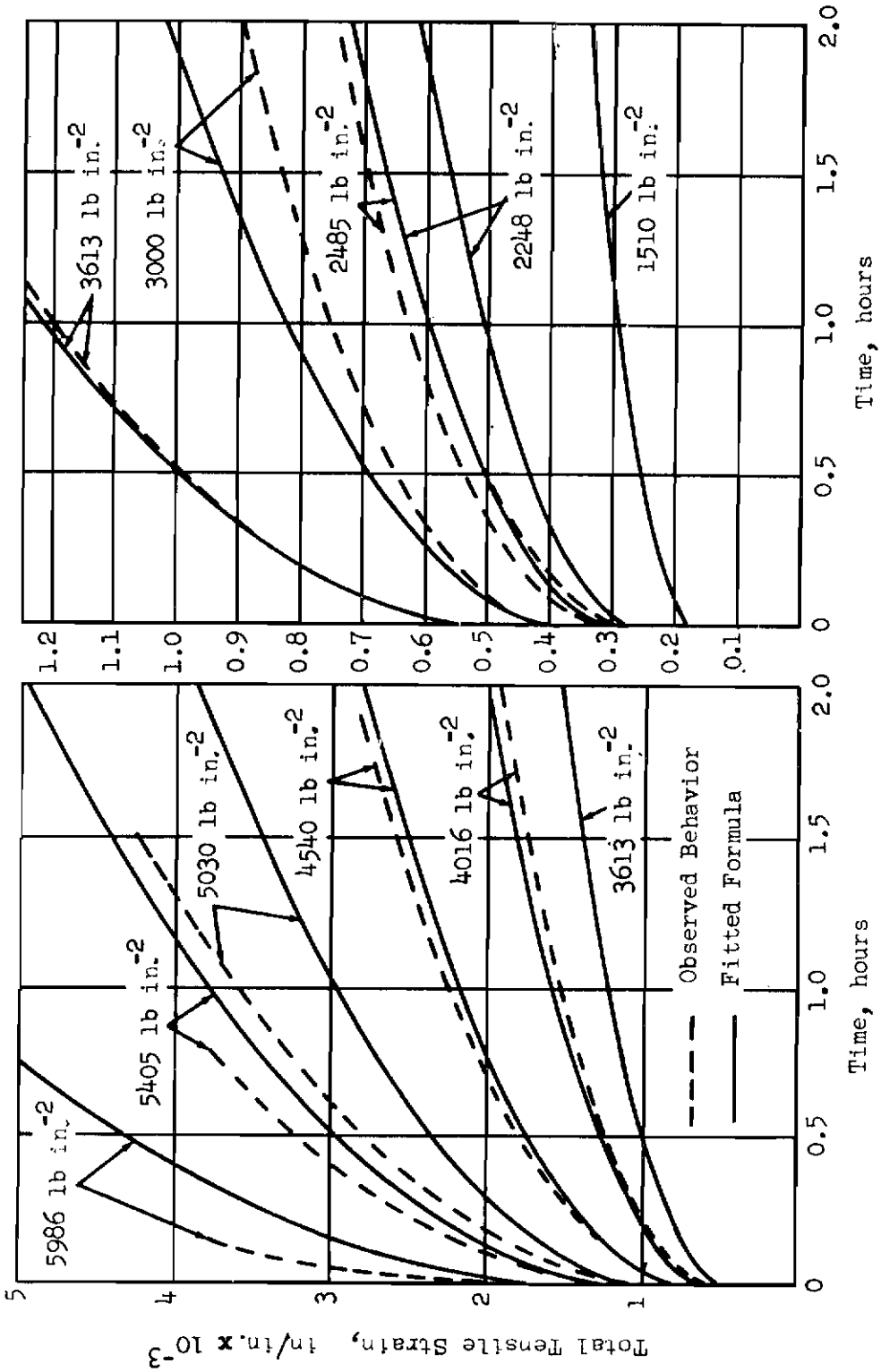

Figure 16. 1100-F Aluminum Time-Dependent Behavior and Fitted Curves (Ref 9)

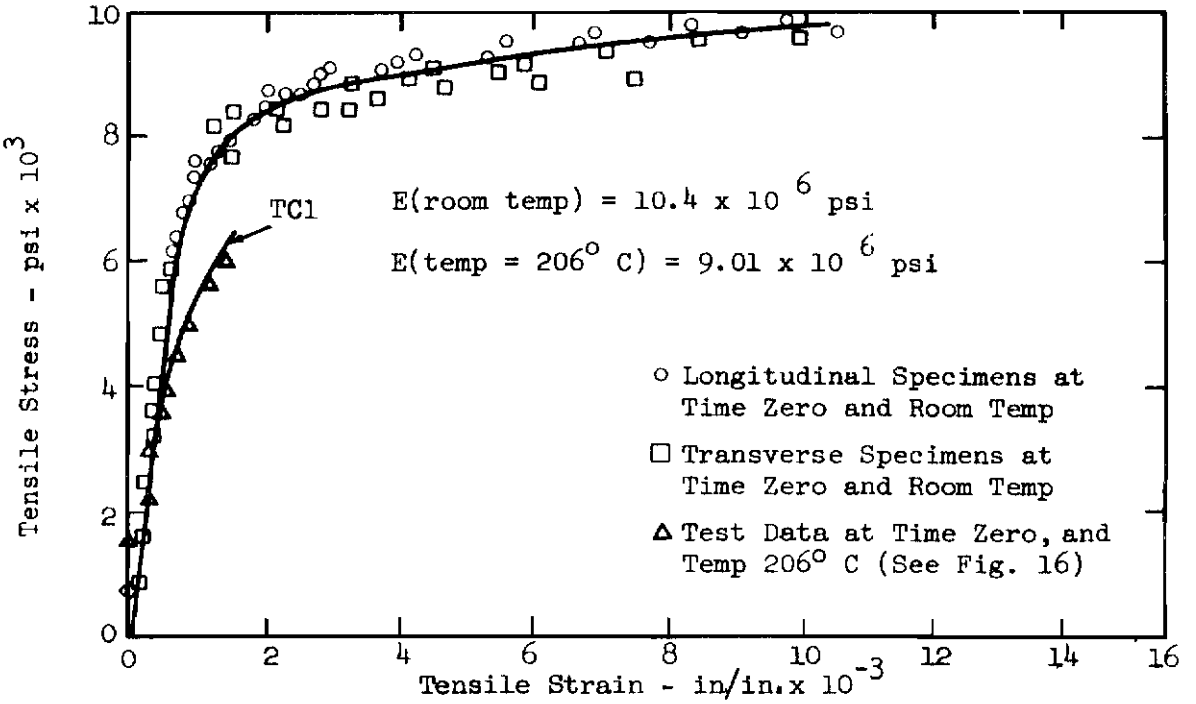

Figure 17. 1100-F Aluminum Stress-Strain Data at Room Temperature and at 206°C., for Time Zero (Reference 9)

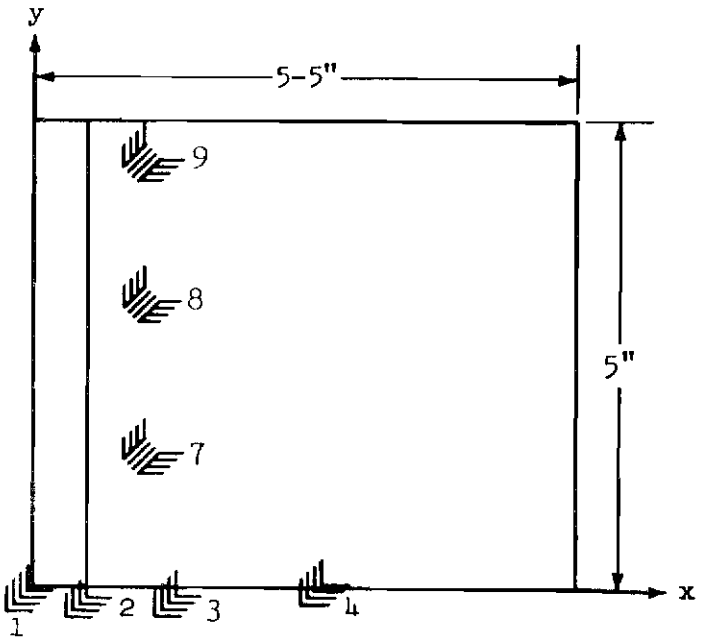

Gage Nos.		Co-ordinates	
Front	Back	x	y
1	11	0.0"	0.0"
2	12	0.5"	0.0"
3	13	1.5"	0.0"
4		3.0"	0.0"
7		1.0"	1.5"
8		1.0"	3.0"
9		1.0"	4.5"

Figure 18. Location of Strain Gages on 1100-F Specimen (Reference 9)

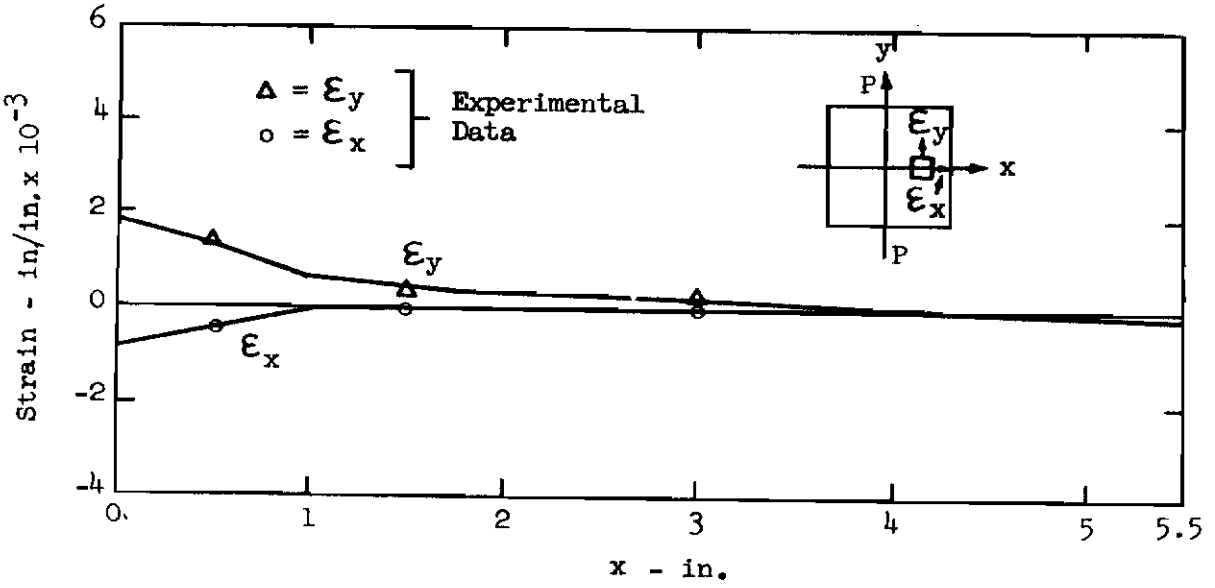

Figure 19a. Strain Distribution on x - Axis for P = 1600# and t = 0.06Hr.

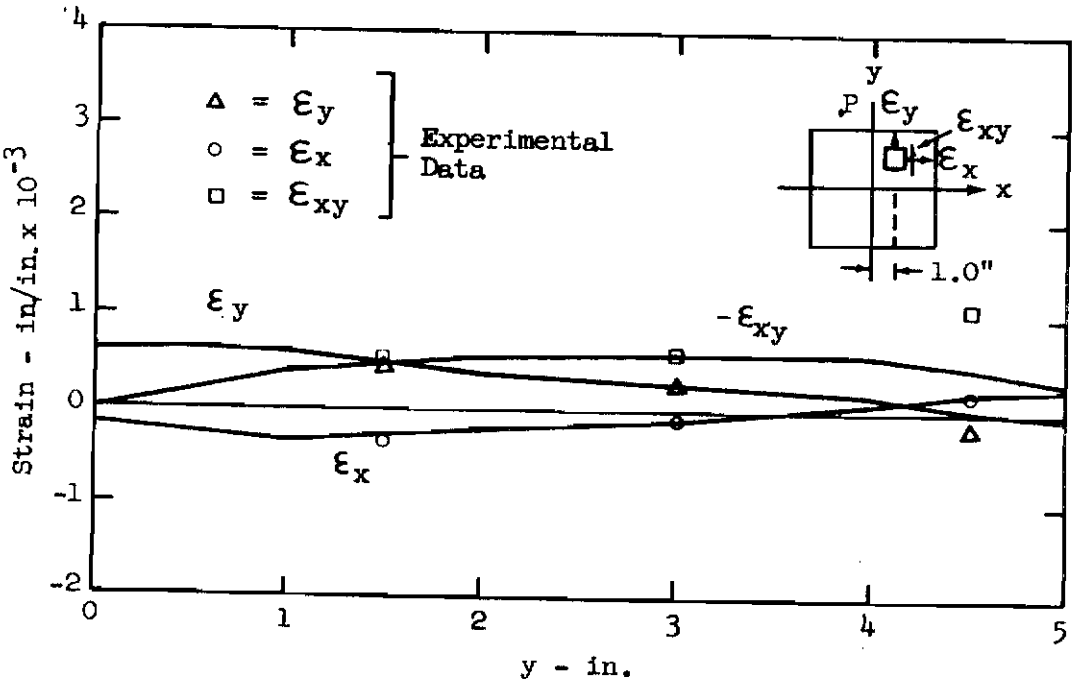

Figure 19b. Strain Distribution on x = 1 for P 1600# and t = 0.06 Hr.

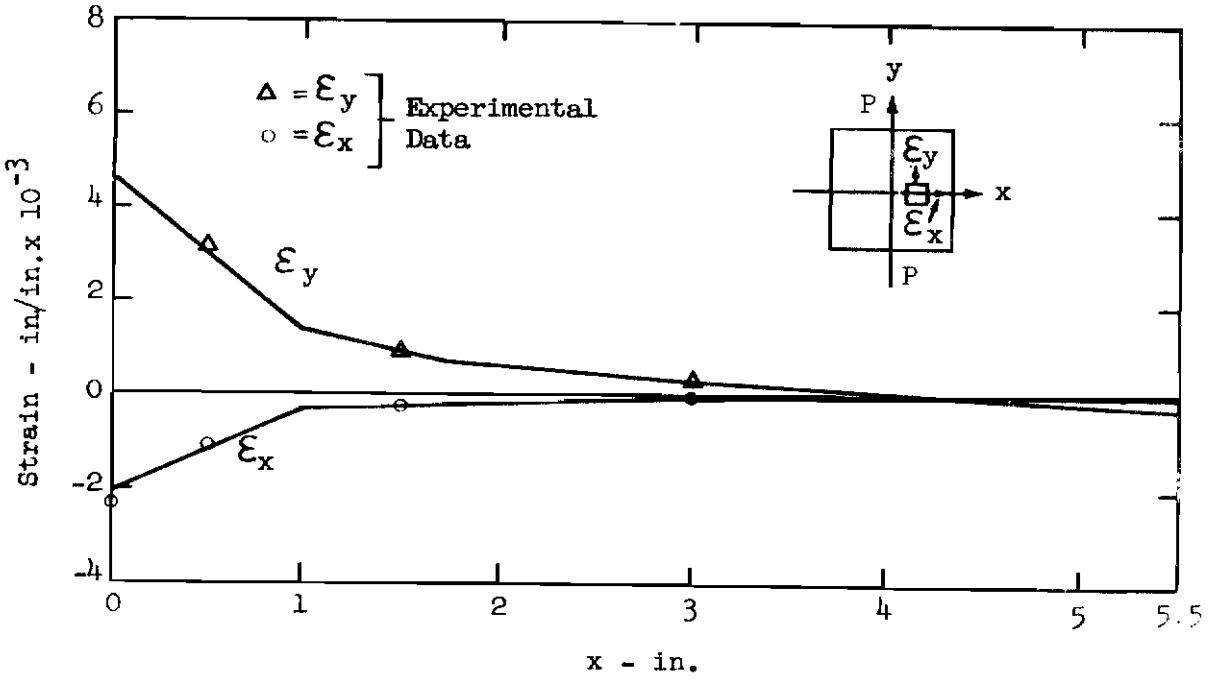

Figure 20a. Strain Distribution on x-Axis for P = 2020 lbs and t = 1.10 Hr.

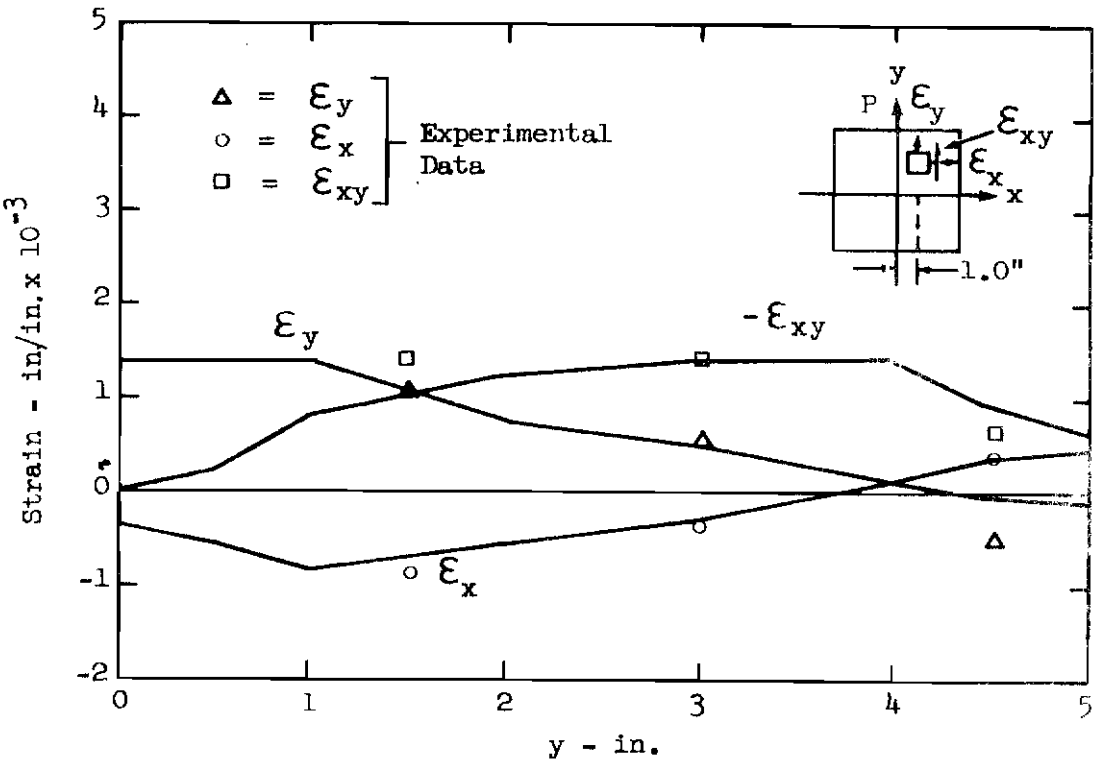

Figure 20b. Strain Distribution on x = 1 in. for P = 2020 lbs. and t = 1.10 Hr.

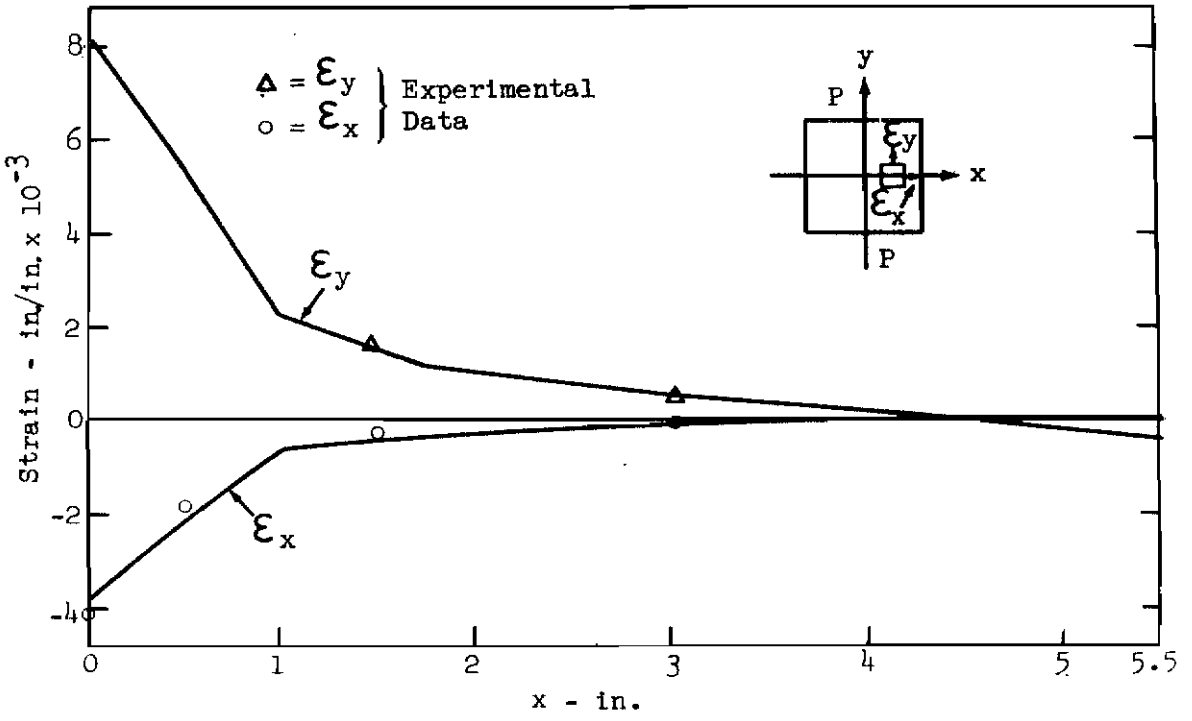

Figure 21a. Strain Distribution on x - Axis for P = 2020 lbs and t = 3 Hr.

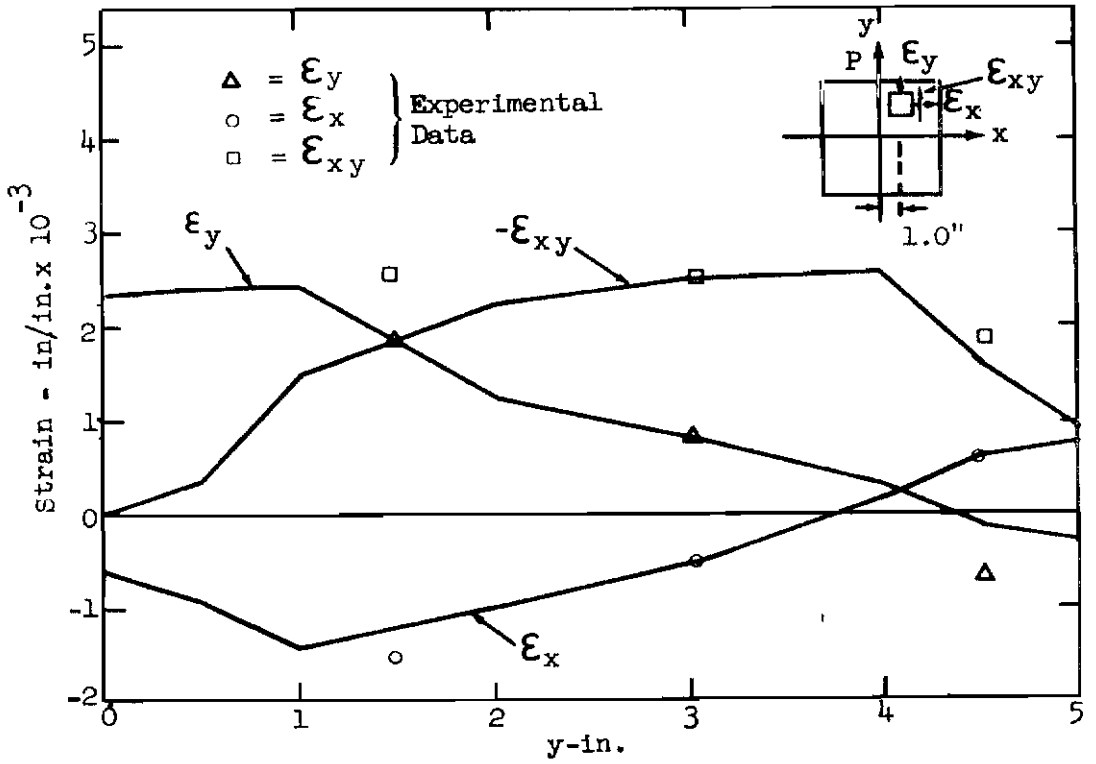

Figure 21b. Strain Distribution on x = 1 in. for P = 2020 lbs and t = 3 Hr.

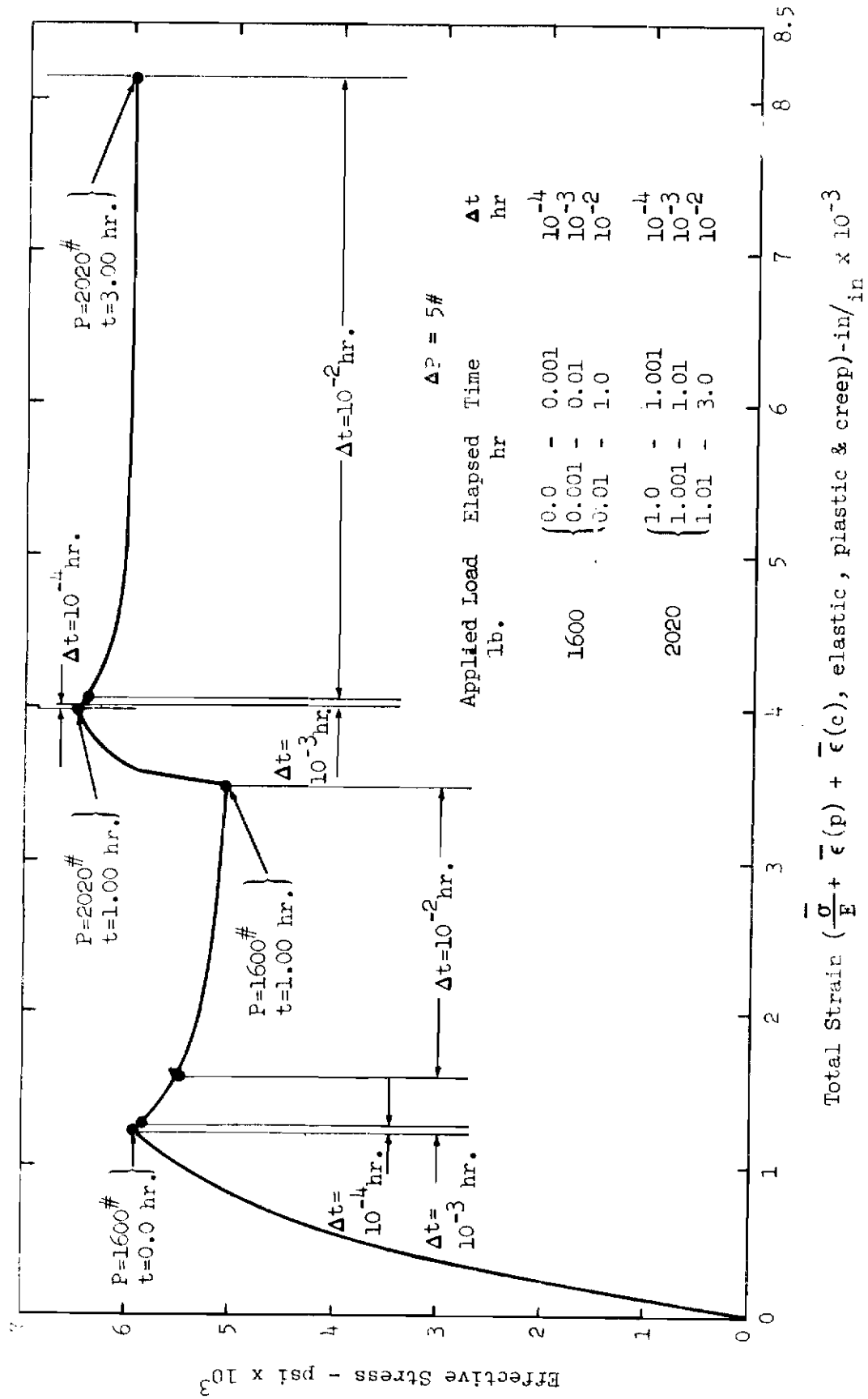

Figure 22. Effective Stress vs Strain at Center Node